Development of a Soft Muscle Actuator Embedded with Sensors

Rancimal Binoy Arumathanthri

(188051T)

Thesis submitted in partial fulfillment of the requirements for the degree Master of Science in Mechanical Engineering

Department of Mechanical Engineering

University of Moratuwa
Sri Lanka

July 2021

DECLARATION

I declare that this is my own work and this dissertation does not incorporate without acknowledgement any material previously submitted for a Degree or Diploma in any other University or institute of higher learning and to the best of my knowledge and belief it does not contain any material previously published or written by another person except where the acknowledgement is made in the text.

Also, I hereby grant to University of Moratuwa the non-exclusive right to reproduce and distribute my dissertation, in whole or in part in print, electronic or other medium. I retain the right to use this content in whole or part in future works (such as articles or books).

Signature: Date:

The above candidate has carried out research for the MSc thesis under my supervision.

Signature of the Supervisor(s): Date:

Dr. K.V.D.S. Chathuranga
Senior Lecturer
Department of Mechanical Engineering
University of Moratuwa

Abstract

Soft robotics plays a vital role in modern day robotics as day by day demand for soft robotic devices increases. To fulfill this demand more research are now focused on soft robotics and soft actuators are one of the main focus area. Soft robotic applications, such as soft robotic exoskeletons, often use pneumatic artificial muscle actuators. Soft robotic systems utilizing pneumatic artificial muscle actuators are a popular area of study as compactness, lightweight, high power-to-weight ratio, and great safety are just a few of the benefits.

Having sensors embedded to this soft muscle actuators are important as it would make close loop control of the actuators possible. Despite the benefits of pneumatic artificial muscles, they lack sensory feedback for controlling force and displacement. To achieve close loop control, sensors are rarely incorporated into the actuator design. The major drawbacks of currently available sensor feedback systems are that they increase weight of the system and, in some circumstances, cause structural deformations.

The design and fabrication of a displacement sensor to use in a novel soft robotic muscle actuator is presented in this study. Several advantages of this actuator and displacement sensor over conventional sensors and soft muscle actuators include ease of manufacture and negligible effect on actuator performance owing to sensor. Furthermore, as compared to soft actuators and sensors that are already available, the proposed soft actuator and sensor are affordable. The displacement of the actuator was determined using a novel inductance sensing approach, allowing closed loop control of the actuator.

The performance of the soft robotic muscle actuator and displacement sensor was evaluated experimentally by the author. The prototype actuator is light in weight (14g) compared to other actuators and has a high strain (65%) and force-to-weight ratio (Capable of lifting 160 times of its self-weight). The dimensions of actuator are 110mm in length and 31mm in width. The sensitivity of the suggested sensor is 0.0022 $\mu H/mm$ and the hysteresis is less than 1.5 percent, with an average error of less than 4%. Controlling the actuator over a square wave as a reference curve using the built-in displacement sensor was used to test and validate feedback control of the actuator. According to the results, this sensor can accurately determine the displacement of the soft muscle actuator and can be employed in a variety of soft robotic applications.

***Keywords*-Soft Robotic Muscle Actuators, Soft Sensors**

DEDICATION

This dissertation is dedicated to my loving parents who always encouraged and motivated me during my ups and downs.

ACKNOWLEDGMENTS

I would like to offer my dearest gratitude to my supervisor, Dr. Damith Chathuranga for providing his support, guidance, encouragement and patient throughout this research. He was a mentor to me than a traditional supervisor who understood my capabilities and provided the required guidance and advises which ultimately made this research a success. I'm highly grateful for dedicating his valuable time on me.

Then I would like to thank Mr. Asitha Kulasekera who always stood behind me throughout this research and provided his insights, subject expertise and guided me towards success. Without him this research might not be a reality. Beside that i like to thank my progress review panel, Dr. Buddhika Jayasekara and Dr. Thilina Lalitharatne who gave their insights and comments on this work throughout the research so that I moved forward in right direction. My lab members in Computational Sensing and Smart Machines Laboratory, Mr. Chanaka, Mr. Lakmal, Mr. Lihini and Mr. Dhanushka deserve a special mention since they helped me a lot in many ways. Also I need to thank Mr. Sanka from bionics laboratory as well.

This research was funded by National Research Council, Sri Lanka Grant No 17-018 and I would like to express my gratitude towards them for providing all the required funding which makes this research a success. All the people in laboratories and workshops in Department of Mechanical Engineering, University of Moratuwa deserve my gratitude for providing their service when ever required without any hesitation.

Finally I would like to thank my parents and my two sisters for keeping faith in me and special thank goes to Mr. Mahesh Gamage who helped me a lot financially throughout these past few years.

TABLE OF CONTENTS

LIST OF FIGURES

LIST OF TABLES

CHAPTER 1

INTRODUCTION

Present trend on robotics shift towards "Soft Robotics" whereby the components of a robot made using softer materials with novel actuation systems compared to traditional robotic actuation. Soft robots have fewer or no rigid materials compared to conventional machines and robots, and are made mostly of softer materials such as rubber, silicone, polymers, or any other easily deformable materials [27]. Rigid robots have the ability to be incredibly powerful and precise, and they are widely utilized in the manufacturing industry [39] and industrial automation. Then again the field of robotic grows beyond manufacturing and industrial automation and move towards healthcare, human assistance and home automation [27]. With this trend conventional robots require complex safety protocols and stability control algorithms to operate around humans or any other fragile workspace while soft robots do not required such complications due to its inherent compliance [50]. Thus soft robots can interact with humans and environment in safer manner where this unique features allows it to have various application areas [26].

Pneumatic artificial muscles widely used in soft robotic applications due to their ability in producing forces and displacements [23] [7]. One such application is using pneumatic artificial muscles (PAMs) as actuators for lower limb robotic exoskeletons [52]. Due to advantages such as compactness, lightweight, high power to weight ratio and high safety, soft robotic systems with PAMs is an immerging topic of interest [10]. First pneumatic artificial muscle design is McKibben type muscle actuator which was introduced in 1950s [7] and currently developed to industrial scale actuators. At present 20cm size McKibben actuator can produce around 3500N [9].

Some of the developments of McKibben muscle are hydraulically actuated McKibben muscle which generate high forces compared to traditional McKibben muscle [32] and most recent development is thin McKibben muscle which have advantages such as high compactness and lightweightness [25]. Other than McKibben muscle recent research is focused on developing pneumatic muscle actuators which are more compact, lightweight and generate high power to weight ratio. Soft Robotic Pad [44], Flat Pneumatic Artificial Muscle [23], Active Support Splint [42] and Pneumatic Artificial Muscles Reinforced by Straight Glass Fibers [34] are few such actuators.

Wearable robotic devices such as robotic exoskeletons made out of pneumatic artificial muscle actuators have become popular due to its unique features such as high safety, light weightness and low mechanical constrains [37]. Such exoskeletons use soft actuators for knee, ankle movements [17] and finger movements [35] etc. However, dimensions of currently available pneumatic artificial muscle actuators are basically cylindrical in shape and trend is to develop flat thin PAMs which are more suitable for wearable devices like robotic exoskeletons.

Despite the benefits of PAMs, feedback for force and displacement control is lacking. To achieve close loop control, sensors are rarely incorporated into the actuator design. However, it should be noted that there are few rigid methods such as obtaining position feedback of PAMs using encoders [7], potentiometers [20], hall effect sensors [5] and semi rigid methods such as getting force feedback using strain sensors [54] and gauge pressure sensing [21]. On the other hand, methods that use conductive liquids as sensors, have been implemented. It was discovered that encapsulating a liquid conductive substance like gallium-indium alloy inside a channel made in the actuator acts as a strain gauge that can be used to measure the actuator's deformation [12] [33]. The major drawbacks of this type of sensor feedback system are that it adds extra weight and, in some cases, causes structural deformations [2].

This research discusses about a soft muscle actuator with a displacement sensor that has a flat low-profile orientation and uses a novel inductive sensing approach. The actuator is actuated by vacuum pressure and contracts longitudinally. The actuator's skeleton is a low-profile spring, and the spring's inductance is used to sense the actuator's displacement.

1.1 Objectives of the Thesis

- Design and develop a soft muscle actuator with an embedded sensor which can measure deformations of the actuator.
- Develop control method to control the mentioned actuator and evaluate the performance of the said soft muscle actuator

A low profile vacuum actuated soft muscle was developed where the low profile skeleton spring is used as displacement sensing element. To feedback control the actuator, a proportional control system was employed, and an experiment was planned and carried out to validate the control system by determining whether the measured value from the feedback is stable. The position signal collected from the displacement sensor was used to implement position feedback.

1.2 Thesis Overview

Altogether this thesis consists of four chapters where chapters are extending as follows. Chapter 1 describe the introduction about this research and the overview of the research. Chapter 2 discuss about the soft muscle actuators available in the research field, their functionality, present trend and their drawbacks. Different types of sensing methods used in soft muscle actuators and different type of materials are discussed as well. Chapter 3 consists of the low profile muscle actuator embedded with sensor design, fabrication and characterization. The Final chapter of the thesis discusses about control system of the soft muscle actuator and validation of the feedback control of the actuator and conclusion of the research.

CHAPTER 2

LITERATURE REVIEW

Literature about soft muscle actuators can be basically categorised into three main topics

1. Types of soft muscle actuators
2. Sensors for soft muscle actuators
3. Materials used for soft muscle actuators

The structure of the literature review can be graphically visualized as below

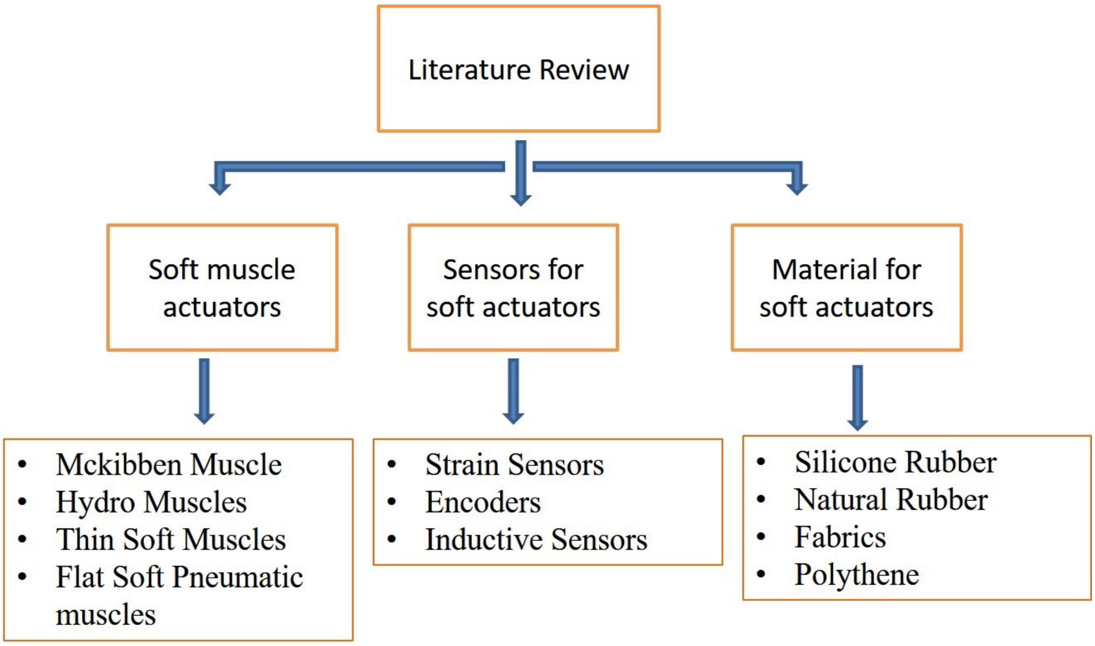

Figure 2.1: Structure of literature review

Since this research is mainly focus to develop a soft muscle actuator embedded with a displacement sensor it is important to get an idea of present trend towards soft robotic muscle actuators, their functionality and drawbacks. Further it is important to get an idea about sensors incorporated for soft muscle actuators as well as materials used for soft muscle actuators.

2.1 Soft Muscle Actuator Types

2.1.1 McKibben Muscle

McKibben pneumatic artificial muscle was developed during two artificial limb researches that were conducted in 1950's and 1960's. McKibben muscles are made up of an internal bladder which is covered by a corded mesh. This shell type outer case of the muscle is attached to fittings or to tendon structure at either end. It tends to expand its volume by pushing its inner surface against the external shell, when the pressure of the gas inside the internal bladder is increased. The actuator gets shortened with the volume increment, because of the very high longitudinal stiffness of threads in the corded mesh. It can produced tension, if it is coupled to a mechanical load. This phenomenon causes characteristics similar to variable stiffness spring in the McKibben muscles. Physical flexibility, light weight and nonlinear passive elasticity are added advantages of the McKibben muscles compared to other artificial actuators [7] [1].

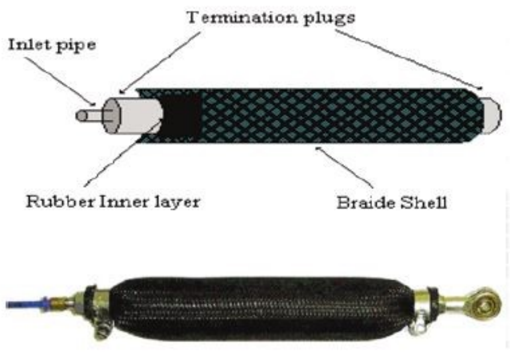

Figure 2.2: McKibben muscle actuator [46]

Chou et al [7] has done a comparison of mechanical properties between McKibben actuators and biological muscle and below figure demonstrate that comparison.

properties	units	McKibben actuators @ 5 bar			Biological muscles
		Nylon shell	Fiberglass shell	Bridgestone	
Resting length (L_o)	cm	14.0	20.0	14.7	
Dynamic range	L_o	0.75 - 1.1	0.86-1.14	0.79 - 1.02	0.64 - 1.12
Maximum tension	N	110 @ 1.1 L_o	56 @ 1.15 L_o	260 @ 1.02 L_o	
Stiffness	N/L_o	314	200	1130	
Work per cycle	NL_o	19	7.8	30	
Cross section area	cm^2	0.95 @ 0.75 L_o	0.64 @ 0.85 L_o	2.0 @ 0.78 L_o	
Tension intensity	N/cm^2	116	88	130	35
Stiffness intensity	$N/L_o cm^2$	331	313	565	73
Work density per cycle	J/cm^3	0.20	0.12	0.15	0.13
Coulomb friction	N	2.5	5	5	0
Maximum velocity	L_o/s	> 6.19			2 - 8 or 20
Average power density	W/cm^3	1.1			
Peak power density	W/cm^3	2.65			0.70
Energy efficiency	-	0.32 - 0.49			0.2 - 0.25

Figure 2.3: McKibben actuators and biological muscle comparison [7]

Theoretical contacting force of Mckibben muscle can be shown using below equation [32]

$$F = (\pi/4)D_0^2 P(1/\sin\theta_0)^2[3(1-\varepsilon)^2\cos^2\theta_0 - 1]$$

Where D_0, P and ε represent the inner diameter of the rubber tube at the initial position of actuator, the applied pressure, contraction ratio, and θ_0 represent the angle of the spiral fibers respectively.

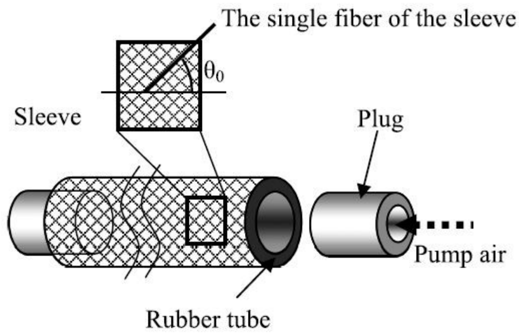

Figure 2.4: McKibben actuator construction [32]

Force comparisons of mckibben muscle with other conventional actuators are as below

	Hydraulic cylinder	Air cylinder	Ball screw	McKibben artificial musle
Mass (kg)[a]	2.79	1.36	5.1	0.29
Stroke (mm)	550	574.0	400	175
Maximum force (N)	439.6	343	684	1650
Volume $\times 10^3$ (mm^3)[a]	494.55	528.07	1698	673.14
Length (mm)	700	700	662	700
Sectional area (mm^2)	$15^2 \times 3.14$	$15.5^2 \times 3.14$	45×57	$17.5^2 \times 3.14$
FDV (N/mm^3)[a]	0.89×10^{-3}	0.65×10^{-3}	0.38×10^{-3}	2.45×10^{-3}
FDM (N/kg)[a]	0.16×10^3	0.25×10^3	0.13×10^3	0.29×10^3
EDV (J/mm^3)[a]	489×10^{-3}	373×10^{-3}	161×10^{-3}	195×10^{-3}
EDM (J/kg)[a]	86.7×10^3	144.8×10^3	53.6×10^3	452.6×10^3

[a] Hydraulic/pneumatic pumps are not included.

Figure 2.5: McKibben actuator comparison (FDV - Force density volume, FDM - Force density per mass, EDV - Energy density per volume, EDm - Energy density per mass) [32]

McKibben actuator has high power weight ratio, low inertia and high compliance capacity. It has the capability of producing contraction forces up to 7000N in a 100g package [8]. When it is compared the contractile force of a PMA with a natural human muscle for a given cross sectional area, the pneumatic muscle actuator has contractile force over 300 N/cm^2 while the same for a natural muscle is 20–40 N/cm^2 [46]. Force generated using mckibben type PMAs are generally vary linearly with applied pneumatic or hydraulic pressure [47].

2.1.2 Hydro Muscle

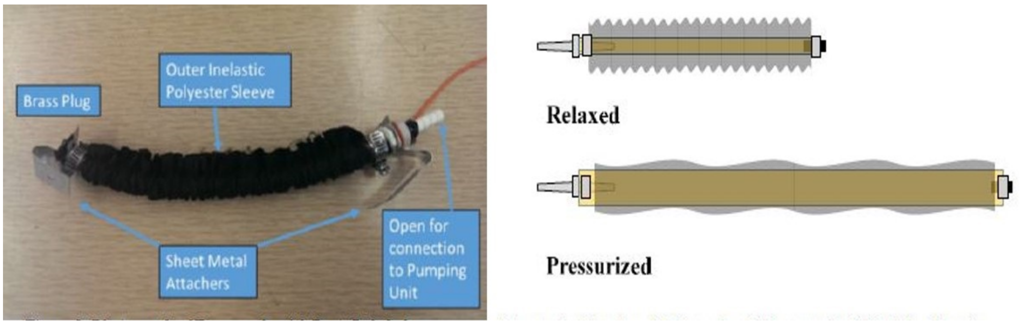

Figure 2.6: Hydro muscle [29]

The requirement of higher number of manageable and independently operated degree of freedom is one of the elementary drawback in mechanical wearable Exo-Musculatures. There are around 800 skeletal muscles within a human body. Every muscles consists of one hundred or more individual motor units [29].

The Hydraulically Actuated Muscle (HAM) Exo-Musculature solves this drawback because it permits for one mechanism, to drive multiple self-actuated and controlled degrees of freedom. There are several benefits of using hydraulically operated Exo-muscles. Fast response time, and smaller energy loss are the two prominent advantages. In addition to that, the higher pressure for incompressible fluid permits packed system design with the same output force [32]. There are two different methods to provide pulling motion, where the hydraulic muscles use elastic potential energy while

McKibben muscles use air pressure. Hydraulically actuated muscles and McKibben muscles operate in opposite manner when it is pressurized. Hydraulically actuated muscles extend for higher pressure while the McKibben muscle contracts. Hydraulic muscle is more efficient and responsive because of the incompressibility of the working fluid. But the McKibben muscle closely mimics the natural muscle [29] [43].

2.1.3 Thin Mckibben Muscle

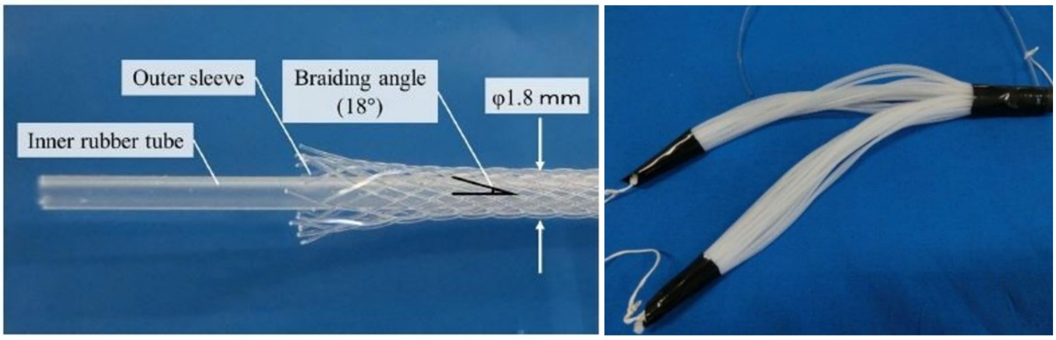

Figure 2.7: Thin Mckibben muscle [25]

This Mckibben muscle has an outer diameter of 1.8mm and weight is 1.3g/m. In applications bundle of this type of muscle is used where each bundle consist of 32 individual muscles to form a multi-filament muscle. When comparing this actuator with conventional pneumatic muscles, this one is more lightweight and compact. Contraction forces and ratios are as below [25].

Design parameters and experimental results for thin McKibben muscle. Muscle Nos. 7, 10, and 12 broke under 0.1 MPa and muscle No. 8 broke under 0.4 MPa.

No.	Hardness [Durometer A]	Angle [deg]	Number of fibers	Max contraction force [N]	Max contraction ratio [%]
No.1	40	30	32	4.06	17.3
No.2	40	20	32	7.86	25.3
No.3	40	18	24	10.05	30.0
No.4	30	30	32	4.17	18.0
No.5	30	20	32	8.61	28.0
No.6	30	20	24	7.67	32.0
No.7	30	20	16	–	–
No.8	30	18	32	15.77	32.0
No.9	30	18	24	10.71	34.0
No.10	30	18	16	–	–
No.11	30	17	32	–	–
No.12	30	17	16	–	–

Figure 2.8: Contraction forces and ratios of thin mckibben muscle configurations [25]

2.1.4 Active Modular Elastomer Sleeve

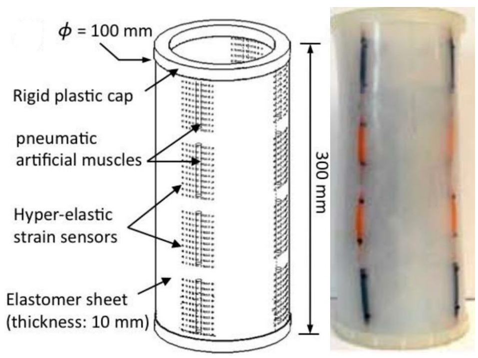

Figure 2.9: Active modular elastomer sleeve [36]

This actuator uses miniaturized Mckibben muscle array. One miniaturized actuator has dimensions of 70mm relaxed length. Each mini muscle can achieve maximum force of 93N. Contraction rate is 25% at 550kPa [36].

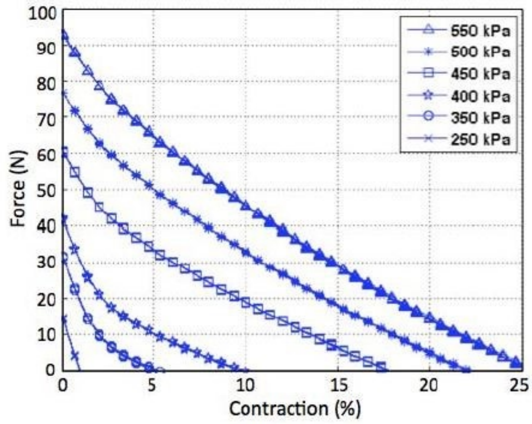

Figure 2.10: Active modular elastomer sleeve characterization [36]

2.1.5 NiTi Spring Actuators

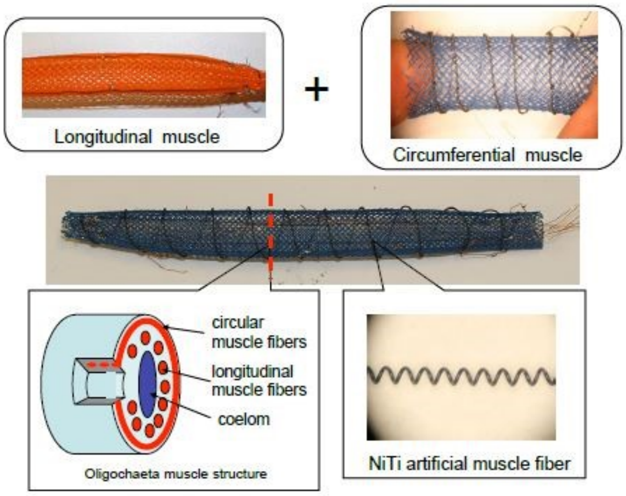

Figure 2.11: NiTi spring actuators [24]

NiTi coil springs are made out from straight wire which is wounded into a coil. In order to reset the memorized shape, the coil is annealed at high temperature. The mechanical properties of NiTi and its performances are depending on the annealing temperature that is used for the reshaping process. If 25 mm long NiTi spring annealed at 390 ℃, it can lift 37.5g weight with stroke length of 50mm. The weight of the NiTi spring actuator is 0.014g, the amount of work done is 0.0184J and therefore the energy density is 1226J/kg [24].

2.1.6 Soft Robotic Pad

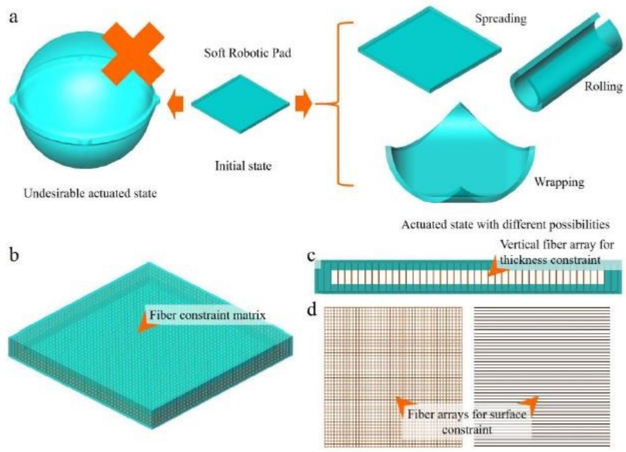

Figure 2.12: Soft robotic pad [44]

A soft robotic pad is a soft pneumatic actuator that can do three different sorts of movements: rolling, saddle, and warping. Simple design is used which uses silicone rubber as fabrication material. In this silicone pad, it contains a thin air pocket to accommodate compressed air which used to actuate the actuator. It can show designated motions such as extending, rolling and bending type motions without any change in thickness. To avoid spherical shaped balloon inflation during actuation different types of constrains used. A vertical fiber array is used for thickness constraint. With only this constraint spreading motion is achieved. The cross and parallel fiber arrays are embedded in the top and bottom layers, respectively, allowing the silicone pad to bend and roll under pressurization.

For fabrication of this actuator layer by layer fabrication method is used where one silicone layer is produced with required constraints in it and then another layer is added to it. The authors used an automated winding machine which produces different fiber patterns that gives required constraints to the actuator.

During SPA testing, bending angles of 90º and 180º showed at 84kPa and 121kPa. Maximum force obtained is 12.4N at 130-140kPa [44]. Fabrication method is complex and not optimized, No embedded sensor included which leads to lack of sensory feedback, applicable as a flat muscle [44].

2.1.7 Flat Pneumatic Artificial Muscle

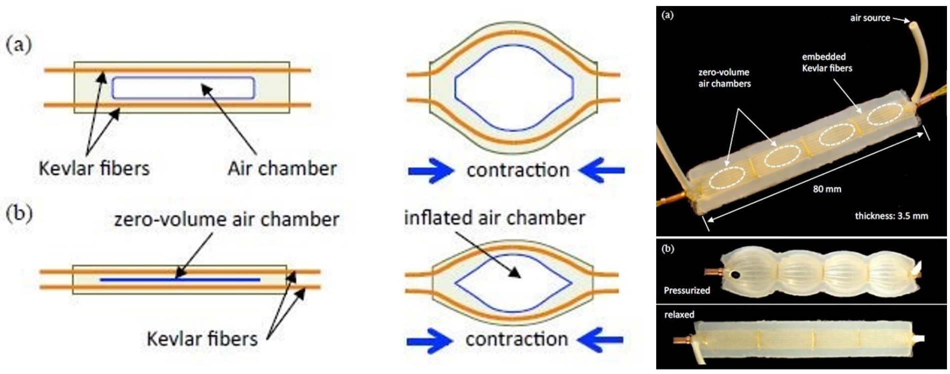

Figure 2.13: Flat pneumatic artificial muscle construction [37]

This flat muscle actuator is consisting of pneumatic elastomer actuators and fabric sleeves. This is a two dimensional design which allows compactness as well as ease in fabrication. In addition it is easily wearable and lightweight. This actuator remains flat in its relaxed state and therefore it is highly compact which is suitable for wearable suits. Additionally, the thickness of the muscle is reduced more than the conventional soft pneumatic actuators by zero volume concept. McKibben muscle, pleated pneumatic muscle and straight fiber embedded rubber muscle are examples for soft pneumatic actuators. The flexible and in-extensible embedded Kevlar fibers compel the circumference of the air chamber. When the air chamber is pressurized, Kevlar fibers generate horizontal contraction force and displacement. There are two different methods to fabricate zero volume actuators. One method is placing a positive mask on the top surface of the cured bottom layer in order to refrain the liquid elastomers from being coated. The other method is applying pattern release sprayed on the unmasked area to prevent top and bottom layers from bonding together.

Results showed that this muscle is capable of generating maximum initial force of 38N and create the contraction displacement up to 18mm for supplied air pressure of 104kPa [37]. Here introducing a sensory feedback system and introduction of fault detection mechanism are few things that can be developed in the future.

2.1.8 Pleated Pneumatic Artificial Muscle

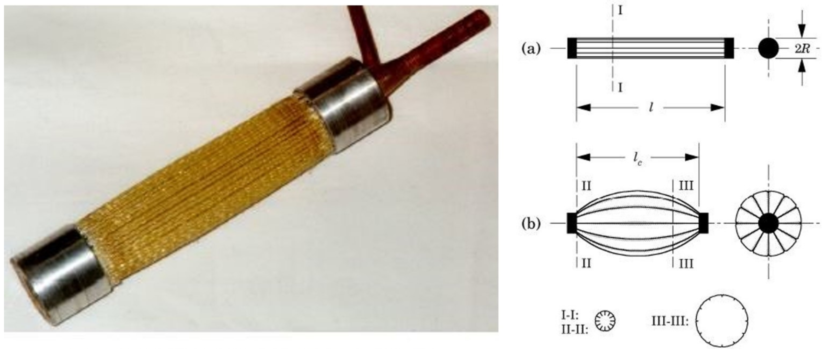

Figure 2.14: Pleated pneumatic artificial muscle construction [10]

The pleated pneumatic artificial muscle is designed to overcome several drawbacks of the braided muscles. Deformation of the rubber tub is one of the disadvantages. The deformation lowers the force generating capability due to its energy requirement. Another considerably important issue is the hysteresis of braided muscles because of the dry friction in between tube and the braid [19]. The design is done with following seven goals, (1) to minimize the deformation of material used for the membrane (2) to eliminate or reduce the friction and hysteresis (3) to have high tensile strength in the lateral axis (4) to have consistent membrane stress (5) low pressure threshold (6) high maximum pressure and (7) high maximum contraction [10].

2.1.9 Straight Fiber Embedded Rubber Muscle

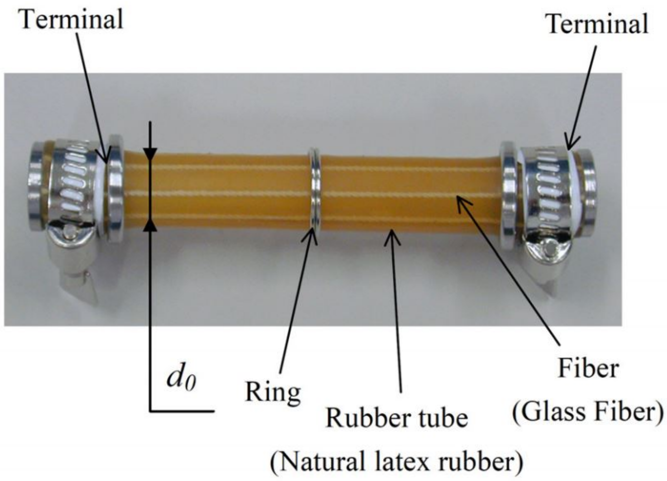

Figure 2.15: Straight fiber embedded rubber muscle [34]

To make straight fiber inserted rubber muscle, high grade carbon fibers are put axially in a tube of rubber. The muscle enlarges by apply of pneumatic force and transforming the change of volume into shrinkage. Since this artificial muscles are reinforced axially by using fiber, the tube's elastic force is the only radial constraint.. Therefore, it is different than McKibben muscles and it can be acquired the contraction force and the elastic deformation of the tube [34]. This actuator consist a length of 72mm and it is 12mm in diameter. The contraction rate of 35 percent or greater generates around 200N of strain under a pressure of 110kPa [40].

2.1.10 Soft Actuator Using Liquid Crystalline Elastomers

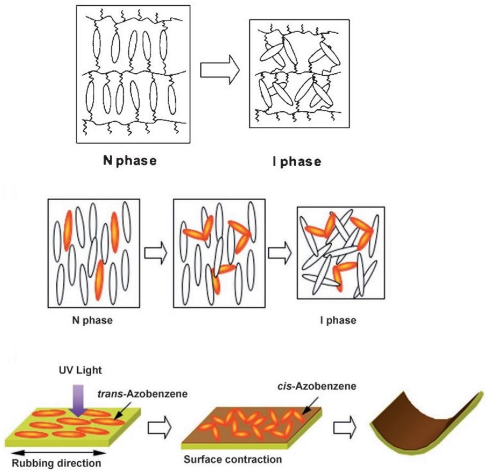

Figure 2.16: Schematic illustration of thermally induced contraction in LCEs [53]

Liquid crystalline elastomers can be use as soft actuators due to their unique combination of the anisotropic features of liquid crystal (LC) phases and the rubber elasticity of polymer networks. It can be used in developing muscle like actuators due to its inherent scalability. Since it responds to light, temperature and electric field, it can be used in vast no of applications in soft robotic field. [4] [53].

2.1.11 Twisted and coiled soft actuator with spandex for artificial muscles

Twisted and coil soft actuators were fabricated using shape memory alloy and polymer fibers. Polymer fibers gained high tensile stroke, large contractile strain, substantial repeatability and low hysteresis. Actuators are comparatively cheaper due to the low cost of used polymers (nylon and polyethylene) [41]. This type of actuator can contract about 34% and generate 2,480 J/kg, which is 64 times greater than mammalian skeletal muscles [18].

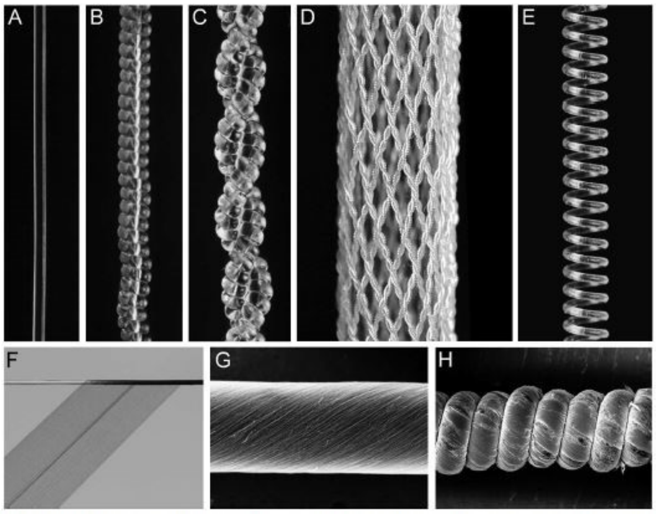

Figure 2.17: Twisted and coiled soft actuator with spandex [22]

2.2 Sensors for Soft Muscle Actuators

2.2.1 Eutectic Gallium-Indium (EGaIn) as Strain Sensor

EGaIn is the most used conductivity liquid in the present generation of soft robotics. Following are the reasons which make EGaIn a good conductive liquid for sensory purposes [11] [51] [3].

(1) Eutectic metal alloy - gallium (75%) and indium (25%) is liquid state @ room temperature (to be used as a conductive liquid in room temperature even though it is an alloy). (2) The resistivity - 29.4×10^{-6} Ω-cm. (Can be used as a contact electrodes). (3) Commercially available. (4) Moldable (Ability to be shaped into free standings while the energy is not minimized). (5) EGaIn is placed on a substrate and the substrate is tilted, gravitational forces cause the EGaIn to redistribute underneath the confines of the skin. (6) Bulk viscosity - 0.002 Pa (Due to low-viscosity it can be used as a thermally stable, electrically conductive lubricant).

The sensor is made up of an elastic rubber matrix with channels of eutectic gallium indium (EGaIn) alloy. When the composite is strained, it contracts in the orthogonal direction and lengthens in the direction of strain. This phenomenon happens according to the materials poisson's ratio. An increment of electrical resistance in the liquid metal channels raised due to the lengthening and contraction that is applied to the channels. This occurrence is taken place due to the geometric principles [30].

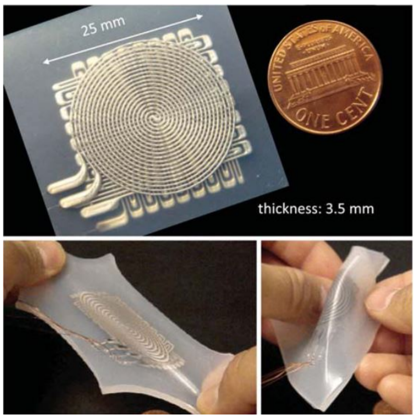

Figure 2.18: Eutectic Gallium-Indium (EGaIn) as strain sensor [51]

2.2.2 Smart Braid Inductance Sensor

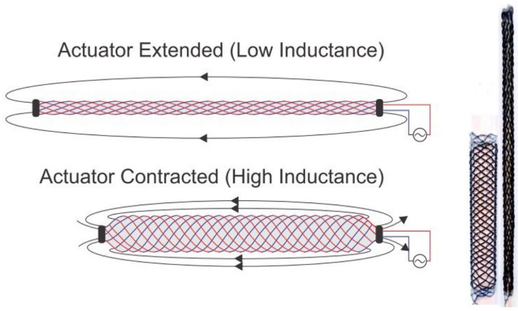

Figure 2.19: Smart braid inductance sensor [14]

Smart braids are fabricated from electrically conductive wires with insulated coating that are connected to form a circuit. Aforementioned conductive fibers are placed alongside with reinforcement fibers in an elastomeric actuator. The motion of the actuator vary the geometry of the smart braid hence change the inductance [15] [16]. Smart braids are simple but effective as it does not respond to environmental conditions such as temperature and inductance value basically vary with the geometry of the circuit only [13].

2.2.3 Soft Displacement Sensor

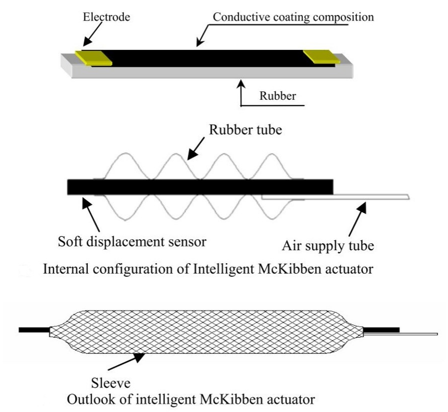

Figure 2.20: Soft displacement sensor [48]

Here Mckibben actuator is integrated with a soft displacement sensor made out of rubber. Sensor is designed with soft material to maintain the high compliance of the actuator. There are basically three types of sensors used for actuators using this concept. Two of these consist of carbon as conductive layer with different thickness and other one uses gold as conductive layer [48] [28] [49].

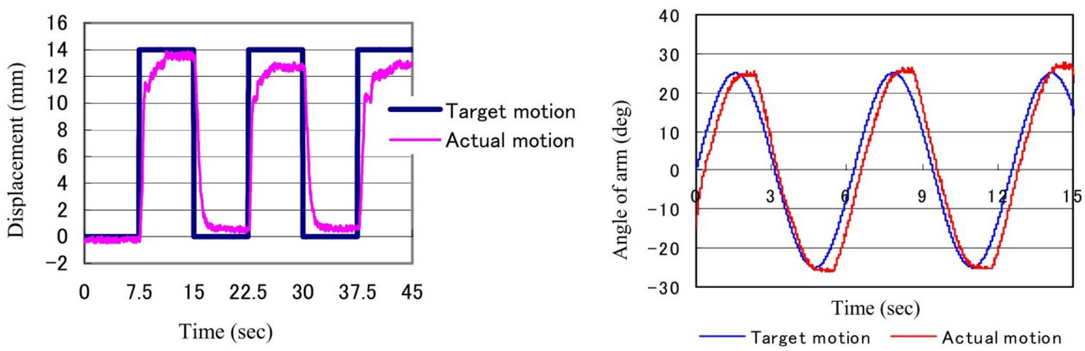

Figure 2.21: Control of actuator using soft displacement sensor [48]

2.3 Soft Material for Soft Muscle Actuators

Soft actuators are made out of highly deformable materials. Most of these materials have low elastic modulus or contain fluids for easy deformation. The main characteristic of these materials and composites are they can be activated and can be produced required motions by external stimuli [22].

To mimic mammalian muscle is one goal in soft muscle actuators and few materials can act as substitute or even outperform the mammalian muscle. Mammalian muscle usually generates approximately 20% strain and 100 kPa stresses, with a work density of 8 kJ/m^3 and power to mass ratio of 50 . At peak performance, mammalian muscle strain can exceed 40%, stress can exceed 0.35 MPa, work density above 40 kJ/m^3 and power to mass ratio above 284 W [31] [38] [22].

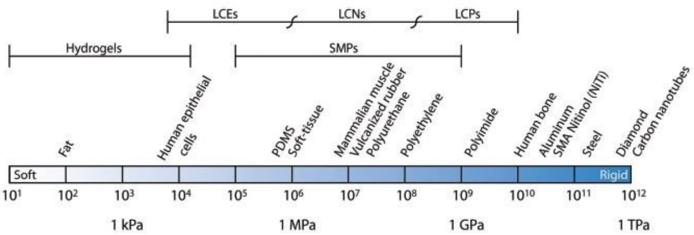

Figure 2.22: Young's modulus comparison of different materials [22]

2.4 Research Gap

Since 1950's soft muscle actuators have been developed although the vacuum type actuation have not been realized. Therefore, the following findings have been found after a detailed literature survey. By literature soft muscle actuator comparison was done as below Table 2.1.

Author	Type of Muscle	Force (N)	Resting Length (mm)	Displacement %	Energy Source	Working pressure	Type of movement
Biological Muscle	N/M	20-40	N/M	35	Chemical	N/M	N/M
F.Daerden 2001	Pleated Muscle	3500	100	41.5	Pneumatic	300kPa	Contracting
N.G. Tsagarakis 2003	Mkibben	300	N/M	35	Pneumatic	600kPa	N/M
S.Wakimoto 2005	Mkibben	5	140	8.6	Pneumatic	400kPa	Contracting
D.Sasaki 2005	Other	20	180	N/M	Pneumatic	0-400kPa	Bending
T.Nakamura 2007	Other	40	80	30	Pneumatic	0-150kPa	Extending
N.Saga 2007	Other	200	72	35	Pneumatic	110kPa	N/M
K.C.Wickramathunge 2010	Mkibben	1000	300	24	Pneumatic	0-500kPa	Contracting
Y.L.Park 2012	Other	90	70	25	Pneumatic	550kPa	N/M
Micheal Wehner 2013	Mkibben	350	200	40	Pneumatic	500kPa	N/M
Y.L.Park 2014	Other	38	80	22.5	Pneumatic	104kPa	N/M
P.Polygerinos 2014	Other	9	N/M	N/M	Pneumatic	350kPa	Bending
F.Z.Low 2015	Other	33.2	250	N/M	Pneumatic	N/M	N/M

S. Sridar 2016	Mkibben	15	N/M	38.5	Hydraulic	N/M	N/M
Kumumaya 2017	Thin Mkibben	15.77	300	34	Pneumatic	0-500kPa	Contracting
Al Fahaam 2017	Mkibben	200	200	30	Pneumatic	400kPa	Extending/Contracting
M. A. Robertson 2017	Other	112	145	N/M	Pneumatic	200kPa	Extending
T.Nakamura 2007	Other	40	80	30	Pneumatic	0-150kPa	Extending
Y Sun 2017	Other	12.4	N/M	N/M	Pneumatic	130kPa	N/M
M.F.Cullinan 2017	Mkibben	3500	195	25	Pneumatic	0-500kPa	Contracting
Al Fahaam 2018	Mkibben	45	160	30	Pneumatic	0-500kPa	Extending/Contracting

Table 2.1: Actuator comparison using literature

In order to identify the research gap below graphical representations were done

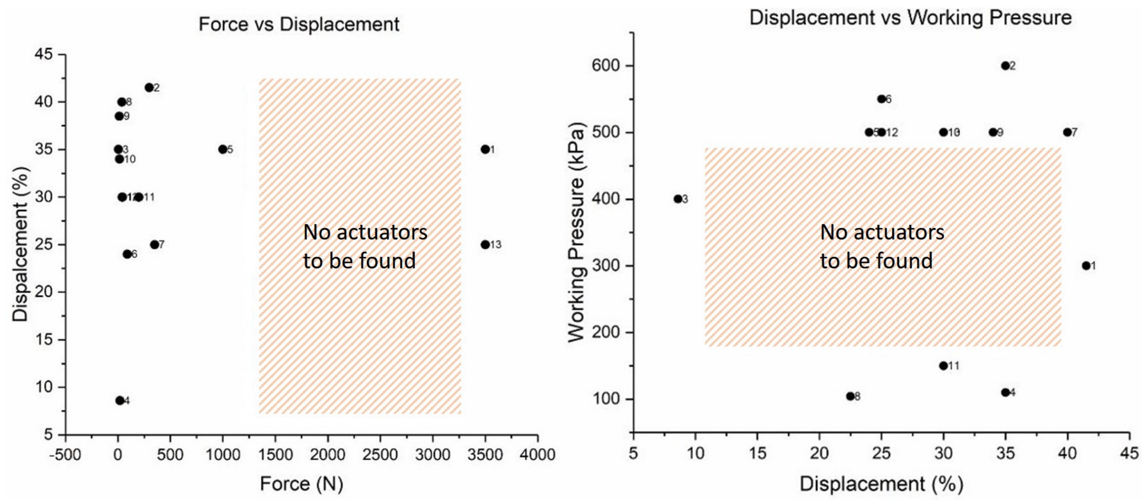

Figure 2.23: Force vs displacement and displacement vs working pressure comparison of available actuators

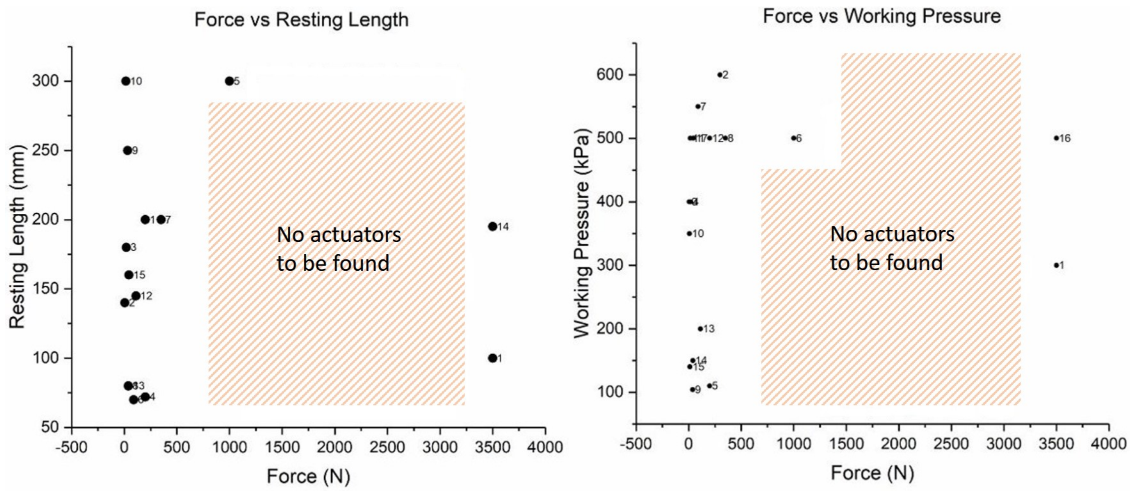

Figure 2.24: Force vs resting length and force vs working pressure comparison of available actuators

According to above data clear literature gap was found and this research is focused on that.

- Less number of research carried out for negative pressure muscle actuators [S.Li et al – 2017].
- Less number of actuators were fabricated for resting lengths between 50mm to 100mm.
- Using graphical representations there are certain areas to be addressed.
- Less number of research carried out for low-profile muscle actuators [Y.L.Park et al – 2014].

CHAPTER 3

METHOD

3.1 Conceptual Design

Low profile spring enclosed vacuum actuator has been proposed for this design. Low profile spring is enclosed using a LDPE film and sealed in order to achieve required deformation. The outer film acts as a container and the inner spring gives shape to the actuator. By applying vacuum to the actuator the air inside the enclosure released and the atmospheric pressure works outside the enclosure to deform the actuator. The relationship between actuator displacement and generated force was modelled as below.

The principle of virtual work is used to derive the relationship between the generated force and the resultant deformation of the actuator. Considering an infinitesimal displacement of the actuator cross-section, the sum of work done by the volume reduction and the resulting spring force is equated to the amount of work done. Here the magazine spring is approximated to a conventional spring model of $F_s = -kx$.

$$FdL + PdV + F_s dL = 0 \tag{1}$$

$$F = -P\frac{dV}{dL} - F_s \tag{2}$$

The differential pressure $P_{atm} - P_{inner}$, is taken as P acting over an infinitesimal volume dV. This differential volume comprises of the multiplication of the cross-section

A by dL. Therefore (2) reduces to;

$$F = -PA - F_s \tag{3}$$

Considering the actuator contraction as positive (upwards when vertically fixed), (3) can be re-written as,

$$F = PA - kL \tag{4}$$

Hence, the generated force per displacement length for a constant spring coefficient depends only on the applied vacuum pressure. The force generated per unit displacement can be increased by the area.This can be done by increasing the cross-sectional area of the actuator or by reducing the spring coefficient. For application in wearable exosuit, the actuator would deliver fixed length actuation. Therefore, the force can be controlled proportional to the applied vacuum pressure.

3.2 Design of the Actuator

The main objective of this actuator is to achieve linear contraction. An effective and uncomplicated design was used to execute this actuation. Flat cuboid shaped design has been selected for this purpose by considering the applications of the actuator. The concept is to make the actuator as thin as possible and generate required forces so that it can be used as an actuator for a soft robotic exoskeleton. Using literature, it is decided to use vacuum pressure (negative pressure) as the working energy for the actuator. Therefore, to achieve the required linear contraction a low profile flat metal spring was enclosed in an in-extensible enclosure design so that once vacuum pressure is given the whole structure collapse linearly and extends vice versa. Furthermore, the flat metal spring helps to regulate the exhaust process and also it helps to maintain the sectional dimensions during contraction of the actuator. As a result of these qualities, the contraction of actuator is more precise. Utilizing a spring makes quick return of the actuator once the vacuum pressure is released , which improves the operating frequency of the actuator and eliminate the requirement of positive pressure line.

The two main parts of the actuator are low profile flat spring which function as a guide skeleton and covering enclosure Fig. 3.1. Guide spring was designed with following dimensions which have 1cm outer diameter in one side and 3cm outer diameter in other side. This dimensions selected using literature to address the identified research gap. To avoid twist and warping of the spring 1.2mm diameter wire has been selected. Total height of the soft muscle actuator is 12cm. The covering enclosure has to be in-extensible and should also be flexible to facilitate the required motion of the actuator.

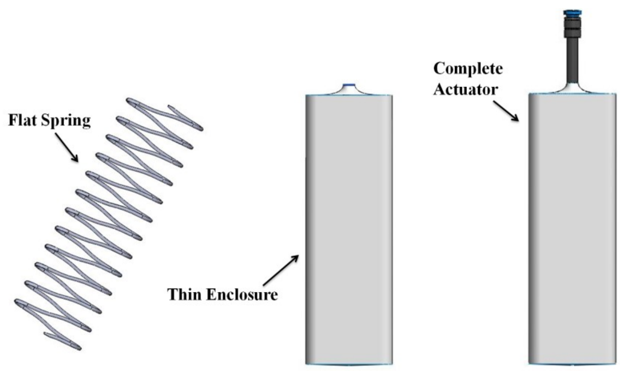

Figure 3.1: Prototype design of low profile actuator

3.3 Design of the Sensor

In a metal spring, inductance is a function of length of the spring. Therefore, by changing the length of the spring, inductance can be varied. A capacitor and inductor can be connected parallel across a voltage source to achieve LC tank circuit. In a LC tank circuit resonance frequency can be achieved by matching the impedance of capacitor and inductor. Hence resonance frequency of a LC tank circuit can be measured using below equation,

$$f_0 = \frac{\omega}{2\pi} = \frac{1}{2\pi\sqrt{LC}}$$

The inductance of a metal spring directly varies with its length. This characteristic of a metal spring can be utilized as a sensor to measure the spring's displacement. Here the inductance value of the low-profile spring was measured using an inductance to digital converter (Texas Instruments-LDC 1614). A capacitor of 1nF is parallelly connected to the metal spring (inductor) to obtain a LC tank circuit. The evaluation module (LDC 1614) is used to measure the oscillation frequency. The evaluation module gives raw data ("DATA") output where it represents the ratio of the sensor frequency (f_{sensor}) with respect to the reference frequency (f_{ref}), in this case 43 Mhz [45]. The sensor frequency is the frequency of which the LC tank oscillates. The ratio is given by:

$$\frac{DATA}{2^{28}} = \frac{f_{sensor}}{f_{ref}} \tag{1}$$

Also

$$f_{sensor} = \frac{1}{2\pi\sqrt{LC}} \tag{2}$$

where"L" is the inductance value and "C" is the capacitor value. By adding the values for equation (1) and (2) it can be simplified to

$$L = \frac{9.69}{DATA^2} * 10^6 \mu H \tag{3}$$

Using equation (3), inductance of the spring was obtained and by plotting inductance vs displacement curve sensor calibration was done.

3.4 Fabrication of the Actuator Embedded with Sensor

A spring has been used as the main structural component for this actuator. Using standard spring manufacturing methods, the obround shaped (low-profile) spring is fabricated, and annealing was used to fix the shape. Two spring materials were used which are mild steel (MS) and galvanized iron (GI). Both galvanized iron and mild steel springs were fabricated using 1.2mm wire, for 11 effective turns over a 100mm length. Other dimensions of the fabricated spring are shown in Fig.3.2. Then two edges of the spring was soldered with thin conductive wires which at the end drawn through the seam of the actuator and connected to LDC 1614 (inductance to digital converter).

Thermal sealing was used to encase the spring inside the LDPE film. First two rectangular shapes were marked in LDPE film. This rectangular shape include dimensions of flat spring, thermal sealing allowance and a pocket to include the LDC 1614 (inductance to digital converter). Once these rectangular shape LDPE film is cut along the markings one seam to seam sealing was done using thermal sealer.

Next the spring was placed inside the two rectangular shaped LDPE films and vacuum line position is marked. Then vacuum line is inserted in one of the film, placed the spring again and remaining three ends were sealed using the thermal sealer. Two conductive wires then drawn through the seam of the actuator. LDC 1614 placed inside the pocket and conductive wires then connected to the LDC 1614. Finally the vacuum line inserted location is sealed using adhesive. Several LDPE film thicknesses were tested to identify the most robust and suitable film thickness. Low thickness film trials have demonstrated low repeatability as they tend to damage the film surface ultimately causing leakages in the actuator. Selected LDPE film thickness was 0.25mm.

3.4.1 Fabrication Method

3.4.2 Fabricated Prototype

Prototype actuator is lightweight (14g) compared to available actuators and has high strain (65%) and force to weight ratio (lifting capacity of 160 times of its self-weight). It is 110mm in length and width is 31mm.

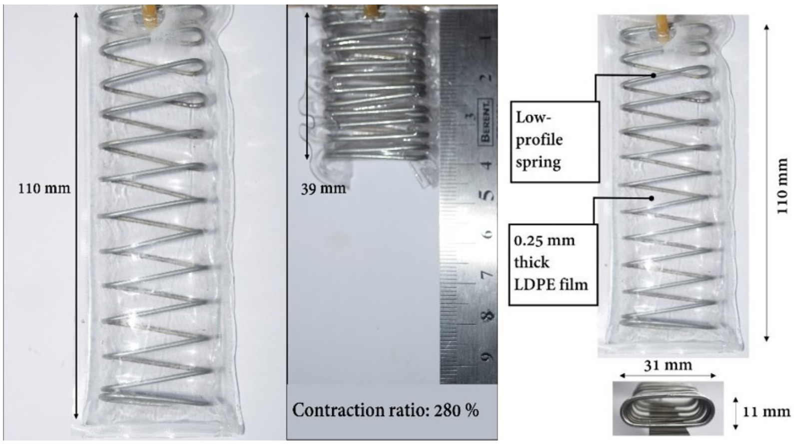

Figure 3.2: Prototype dimensions and contraction ratio

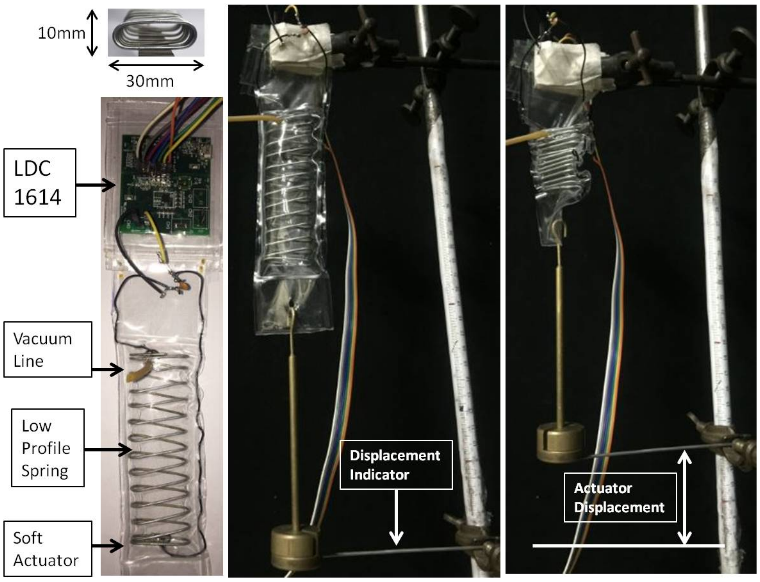

Figure 3.3: Prototype actuator

CHAPTER 4

CHARACTERIZATION OF ACTUATOR

4.1 Experiment to Select Skeleton Spring Material of the Actuator

The behavior of the low-profile spring differs from that of common circular helical spring. The deflection of the spring under axial load and developed stresses are different due to the obround (stadium) cross-section in the selected low profile spring [6]. Therefore, preliminary experiments were carried out to assess the force-displacement characteristics of the low-profile spring. Results shown in Fig.4.1, indicate that it is within reach to assume a conventional spring model of Fs = -kx for this low-profile actuator as well.

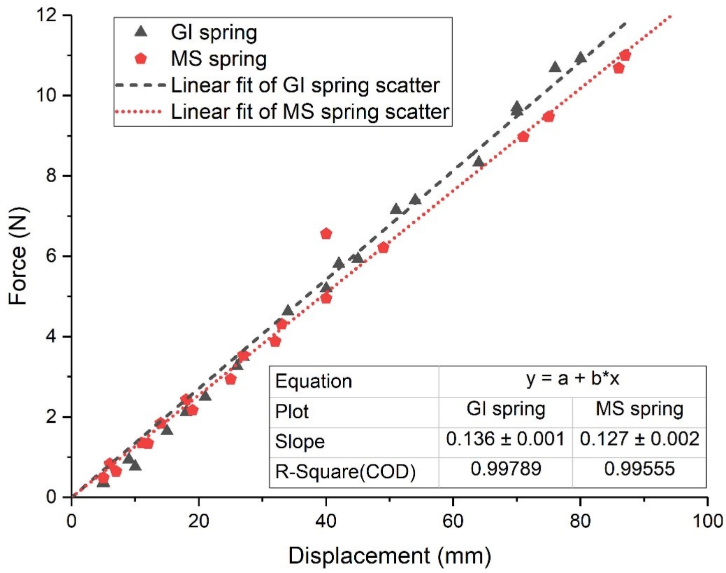

Figure 4.1: Experimental force-displacement curve for GI and MS low-profile springs

4.2 Experimental Setup for Actuator Characterization

An experimental setup was used to characterize the developed vacuum actuator as shown in Fig.4.2. The test setup consist of a vacuum chamber, a vacuum pump, pressure relief valves, a digital scale, set of weights and an actuator holding stand. The vacuum pump used to generate vacuum and vacuum chamber stored the required vacuum for different experiments. Set of weights used as negative force to measure the generated lifting force by the actuator and was measured using digital scale.

Preliminary experiments were performed to identify the spring coefficient of the low-profile spring. Then, tests were carried out to find the maximum force variation with applied vacuum pressure, maximum displacement for a given load with applied vacuum pressure and force-displacement characteristics. The following experiments were repeated for two types of actuators, comprising GI and MS springs.

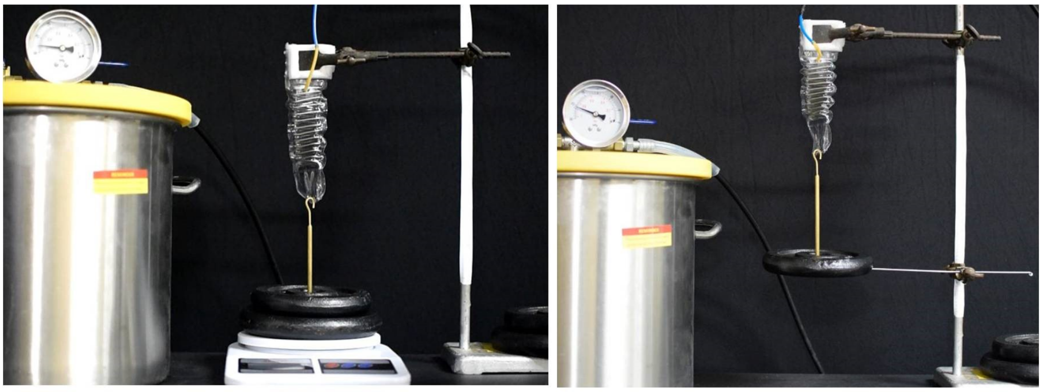

(a) Maximum Force Test **(b) Maximum Contraction Test**

Figure 4.2: Experimental setup for actuator characterization

Generated force vs vacuum pressure, displacement vs vacuum pressure and change in force and displacement with vacuum pressure was plotted using experimental data.

4.3 Experiment to Identify Maximum Displacement Variation of the Actuator

The experimental setup as in Fig.4.2 was used to determine the maximum displacement characteristics of the low profile actuator. A 200 g mass was fixed to a setup similar to previously described. Results were recorded and the displacement vs applied vacuum pressure graph was plotted. Fig.4.3 present the results.

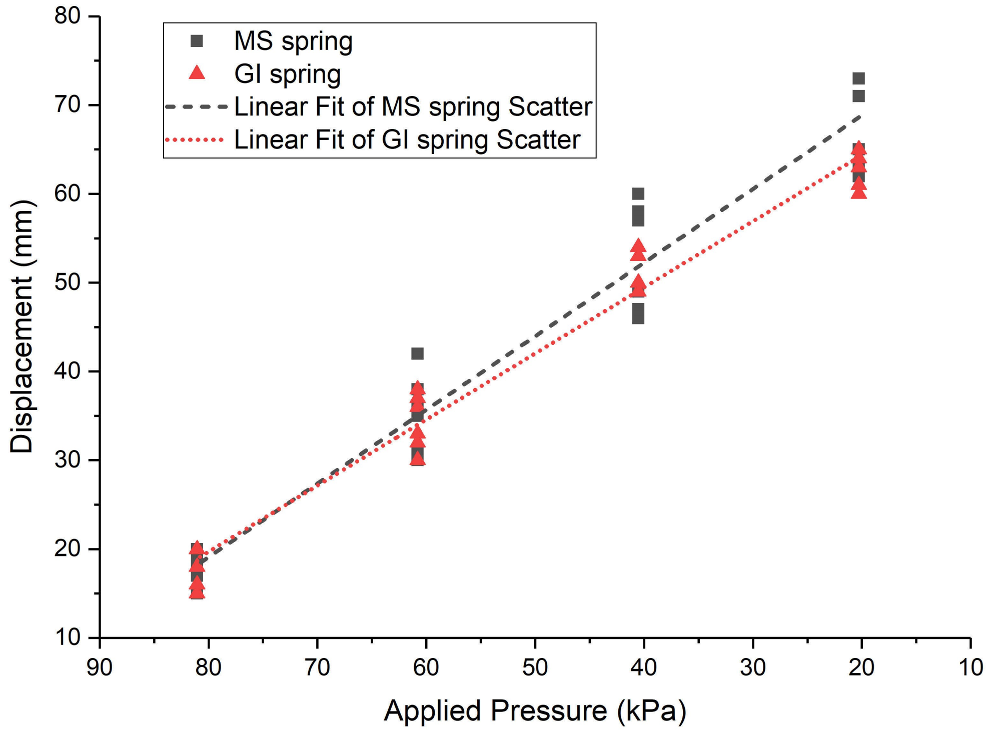

Figure 4.3: Displacement vs applied vacuum pressure graph for actuators with galvanized iron (GI) spring and mild steel (MS) spring

4.4 Experiment to Identify the Maximum Force Characteristics of the Actuator

The experimental setup as in Fig.4.2 was used to determine the variation of maximum force with applied vacuum pressure. A boss head was used to mount an actuator to the frame. Initially a 3.3kg weight was kept at the scale and tare the scale. Then vacuum pressure was applied and maximum negative reading was measured which corresponds to maximum force per given vacuum pressure. Fig.4.4 preset the results.

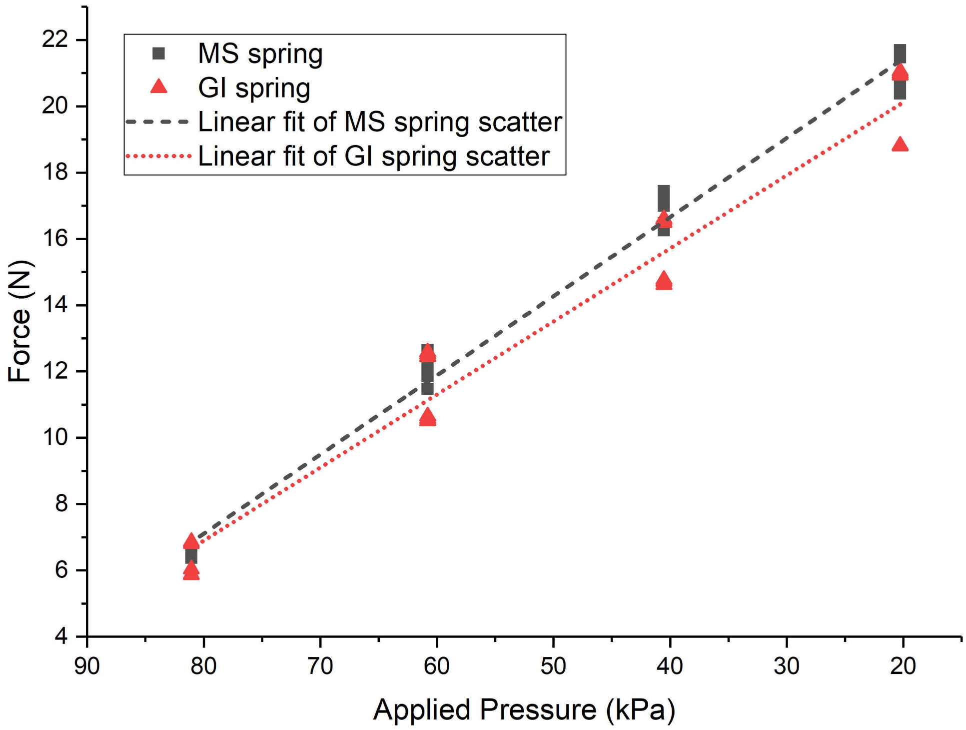

Figure 4.4: Generated force vs applied vacuum pressure graph for actuators with galvanized iron (GI) spring and mild steel (MS) spring.

4.5 Experiment to Identify the Force vs Displacement Behavior of the Actuator

Similar experimental setup (Fig.4.2) as above was used and an isobaric test was performed to determine the force-displacement behavior of the actuator. Vacuum pressure and attached loads were varied and the resultant displacement was recorded using the readings given by the scale. Fig.4.5 preset the results for this experiment.

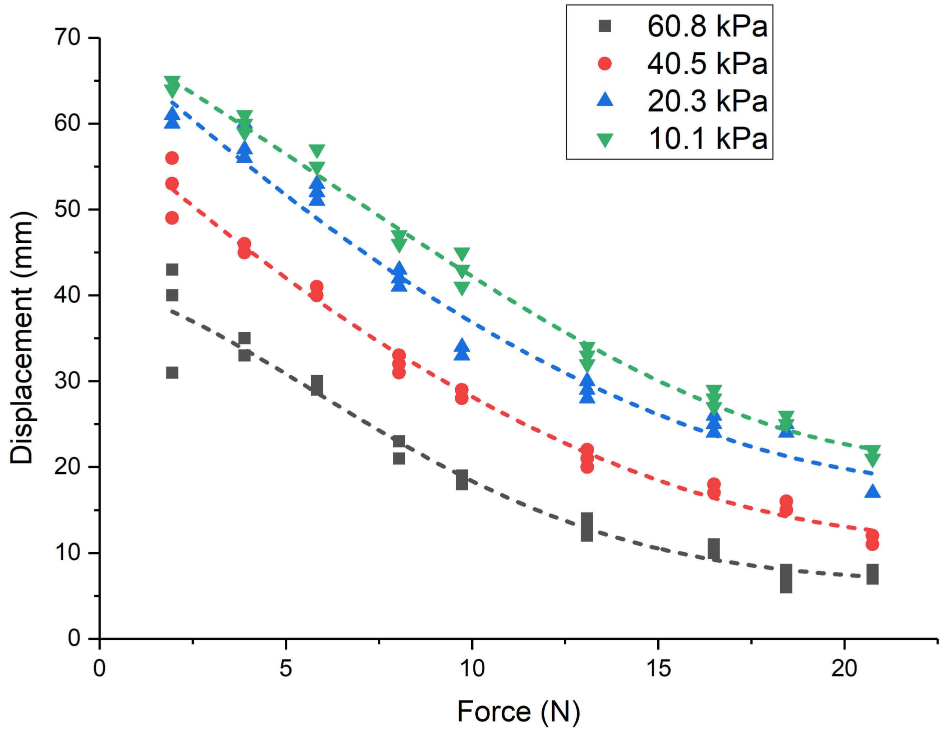

Figure 4.5: Displacement vs generated force for different applied pressures

CHAPTER 5

CHARACTERIZATION OF THE SENSOR

5.1 Experimental Setup for Sensor Characterization

A test setup was used to characterize the proposed displacement sensor. It consists of a vacuum chamber, A vacuum pump, an arduino mega 2560, a motor controller (L298), two solenoid operated flow control valves (FCVs), known weights and a 12V power supply. First, the characterization of the soft muscle actuator with sensor was performed and the same test setup was used to calibrate the displacement sensor. Finally the characteristics of the sensor such as sensitivity, resolution, hysteresis, and repeatability were obtained.

A proportional control system was used to achieve the feedback control of the actuator. Control system was implemented using above mention equipments. To apply and release vacuum pressure independently, each solenoid operated flow control valve set to operate individually. Feedback signal was taken from the inductance to digital converter (Texas Instruments-LDC 1614) and arduino mega 2560 was used to process that data and control the FCVs accordingly. Actuator and actuator embedded with sensor was characterized separately using two different control steps. First soft muscle actuator alone was characterized to identify its behavior and then the complete system consist of actuator with embedded sensor was characterized by implementing aforementioned control system. Fig.5.1 present the relative block diagram.

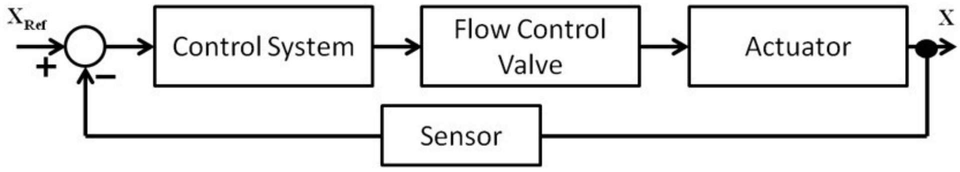

Figure 5.1: Control block diagram of the system

5.2 Displacement Sensor Calibration

The calibration process of the sensor was carried out by recording the inductance values of the spring for different displacements of the actuator and they are graphically represented in Fig. 5.2.

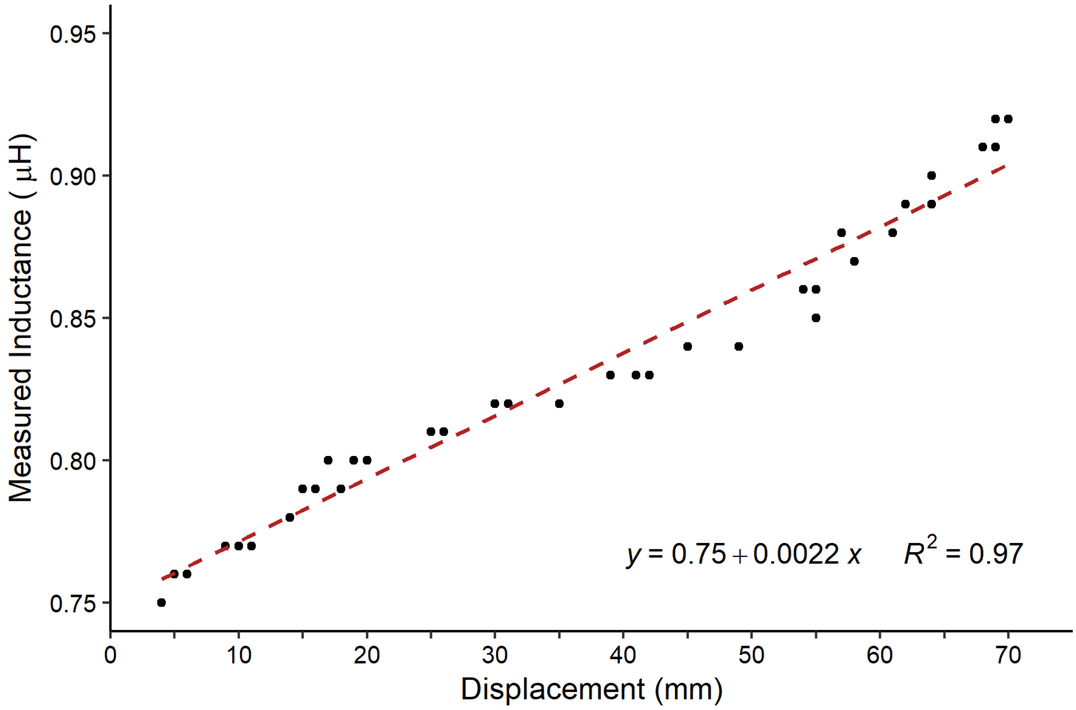

Figure 5.2: Inductance vs displacement curve

A linear relationship between the inductance (L) vs displacement (D) can be acquired from the plot by considering the effective region of the actuator. The linear relationship is expressed using following equation (4).

$$L = 0.0022D + 0.75 \tag{4}$$

5.3 Hysteresis of the Displacement Sensor

The hysteresis of the sensor was determined using loading and unloading curve. Displacement of the actuator was increased and decreased by fluctuating the vacuum pressure inside the actuator and inductance values were measured for the varied displacement values. Then they are graphically represented to find out the hysteresis. The results are shown in the Fig. 5.3 and Table 5.2.

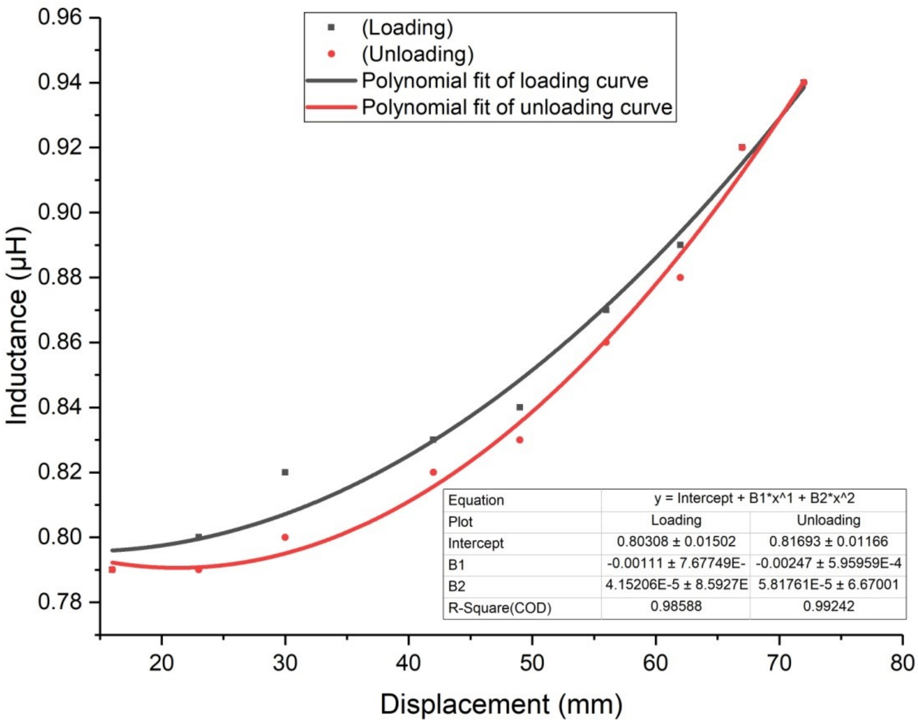

Figure 5.3: Loading and unloading curve

5.4 Repeatability of the Sensor

The repeatability property of the sensor was determined by plotting the sensor readings over twenty iterations for three fixed displacements. The results are shown in Fig.5.4.

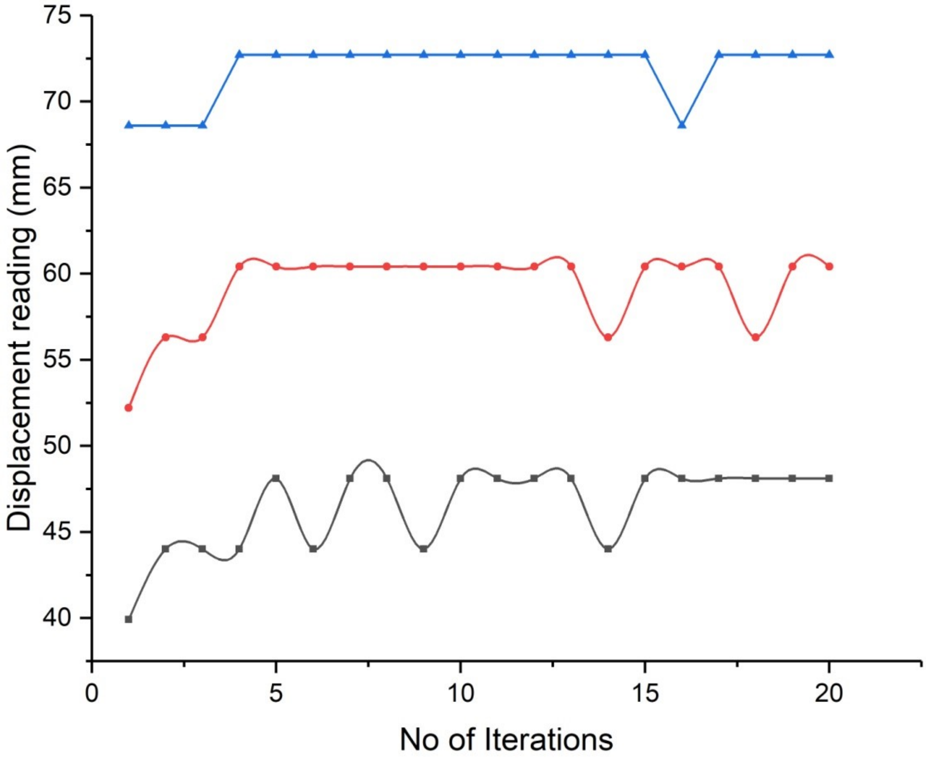

Figure 5.4: Repeatability curve

5.5 Sensitivity, Resolution and Average Error of the Sensor

The characteristic curve of the sensor was used to determine the sensitivity and resolution of the sensor (Fig.5.2). The resolution of the sensor is calculated as 4.09mm/10nH and the gradient of the graph depicts the sensitivity as 0.0022 μH/mm. The experimental data was used to calculate the average error of the sensor and the results are shown in Table 5.1. Overall characteristics of the displacement sensor are shown in Table 5.2.

Table 5.1: Sensor error evaluation

Sensor Output Displacement (mm)	Actual Actuator Displacement (mm)	Percentage Error (%)
27.62	26	6.24
46.48	44	5.62
39.92	41	2.63
59.18	58	2.03
60.41	62	2.56
71.89	69	4.18
Average Error		3.88

Table 5.2: Overall characteristics of displacement sensor

Sensitivity	0.0022 $\mu H/mm$
Resolution	4.09mm per 10nH
Hysteresis	1.49 %
Average Error	3.88 %

CHAPTER 6

VALIDATION OF THE SYSTEM: CASE STUDY

To find out the stability of the feedback system and validity of the control system, an experiment was designed and conducted. Experimental setup used for sensor characterization was used for this as well (Fig.6.1 and Fig.6.2). Position feedback from the displacement sensor was used as correction signal. Input for the system was a 20mm amplitude and 0.25 hz frequency square wave which used as position reference signal. The actual actuator displacement was taken using a camera setup where data taken from the camera was used to get the actual displacement using kinovea video analyzer. Then the reference curve, sensor feedback curve, and actual actuator displacement curve were compared using graphical representation to validate the control system.

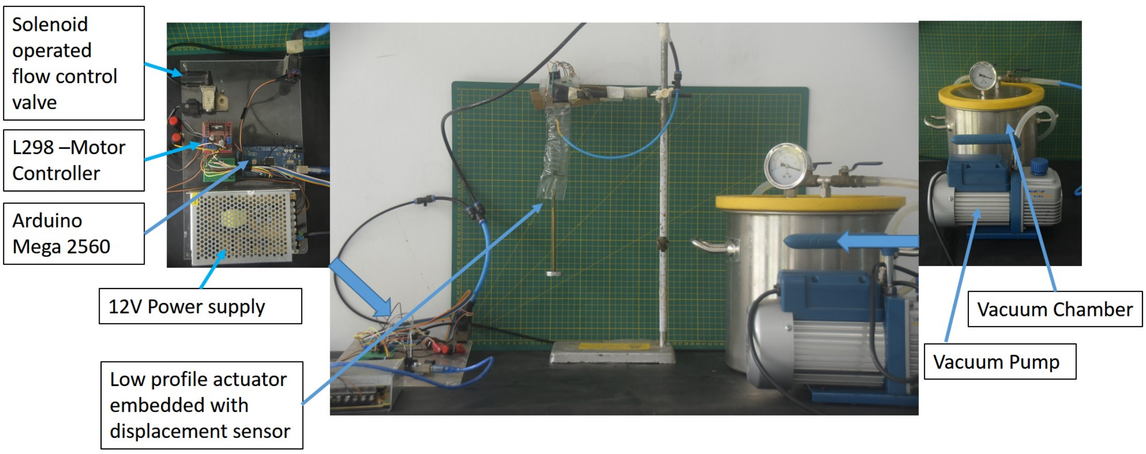

Figure 6.1: Experimental setup for measuring actuator displacement

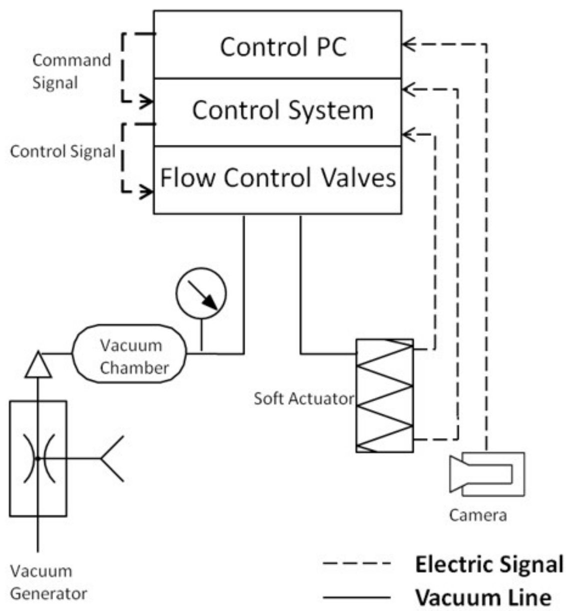

Figure 6.2: Schematic diagram of experimental setup for measuring actuator displacement

Raw data was taken from LDC1614 which provides inductance of the embedded metal spring according to equation (3). The corresponding displacement value was calculated using characteristic equation of the sensor (L = 0.0022D + 0.75). A square wave was given as reference point for this experiment and to avoid displacement limits of the actuator an upper and lower threshold values were defined. Then sensor provided displacement value and reference value was compared and error was adjusted by applying and releasing vacuum pressure to the actuator using solenoid operated flow control valves. The required motion pattern was obtained using this algorithm (algorithm 1).

Results from this experiment are graphically represented in the Fig.6.3. The blue curve represents the input square wave, red curve represents the sensor feedback signal and black curve demonstrate the actual displacement of the sensor which was taken by analyzing the video data using kinovea video analyzer. By going through the Fig.6.3 it can be seen that drift between input and output curves are insignificant where system provides satisfactory position control for the actuator. Therefore, the embedded sensor can be used as a successful displacement sensor for this given actuator.

Algorithm 1 Feedback Control

Set_Point ← Position input signal (sine wave)
Up_thresh ← Upper threshold value
Low_thresh ← Lower threshold value
Feedback_value ← Feedback displacement value
Valve_1 ← Vacuum input valve
Valve_2 ← Exaust valve
if (Feedback_value $\geqslant Set\_Point + Up\_thresh$) **then**
    $Valve\_1 = ON$
    $Valve\_2 = OFF$
else if (Feedback_value $\leqslant Set\_Point + Low\_thresh$) **then**
    $Valve\_1 = OFF$
    $Valve\_2 = ON$
else
    $Valve\_1 = OFF$
    $Valve\_2 = OFF$

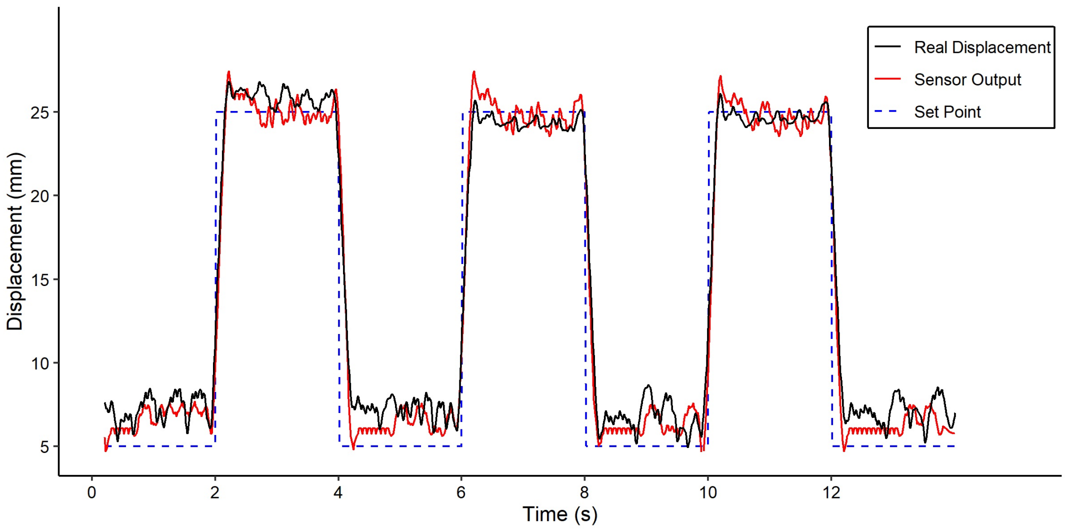

Figure 6.3: Results of position control experiment

CHAPTER 7

CONCLUSIONS

Despite the growing demand for soft robotic actuators, the absence of accurate sensory feedback systems remains a serious challenge. This problem is addressed in this study with an unique displacement sensor integrated into a soft muscle actuator, which yields promising results. The actuator is light in weight (14g), has a powerful lifting force (160 times its own weight), has high strain (65%), and a low profile, and the suggested sensor has no effect on these characteristics or the actuator's performance. The actuator does not require positive pressure for extension after actuation because it has a return mechanism (an enclosed spring). In comparison to existing soft muscle actuators with sensory feedback, fabrication of the actuator and sensor is straightforward and inexpensive. This proposed sensor allows the actuator to work at various displacements and pressure levels, which will be useful in the future.

Even though the inductance of a spring does not behave linearly with displacement, the sensor itself behaved linearly with a small margin of error in the actuator's operating region. According to the results of the experiments it can be seen that repeatability varies at first, but settles over time. This effect is related to the properties of the actuator where due to the characteristics of enclosing polythene the contraction of the actuator improves slightly over time. Hysteresis is 1.49%. Sensitivity and resolution are 0.0022 μH/mm and 4.09mm per 10 nH respectively. These data suggest that the sensor can be utilized for this actuator with a narrow margin of error, as the sensor's average error is 3.88%. The experimental results of the feedback control system suggest that it can be utilized for actuator position control, allowing it to be used in the target application, which is a soft exo-suit. As a result, this actuator can function without the use of external position sensors.

The concept, design, and development of an innovative displacement sensor for a soft muscle actuator are discussed in this research. With regard to this research it can be concluded that this sensor can be successfully used for the intended application under the given environmental conditions after analyzing the sensor's properties and feedback control of the actuator. However, there is one significant drawback. Because this sensor relies on the inductance of a spring to compute actuator displacement, results may be affected by high magnetic fields in the workplace. As a result, it can't be used in such situations. However, because the authors want to employ the actuator as part of a wearable system, this constraint does not appear to be a major concern.

The feedback control mechanism will be improved in the future to achieve more accurate control of the soft muscle actuator. This is accomplished by incorporating a vacuum pressure signal into the system. The mentioned soft muscle actuator will also be miniaturized in order to be used in more complicated applications.

LIST OF PUBLICATIONS

1. R. B. Arumathanthri, A. L. Kulasekera, and D. S. Chathuranga, “An Induction Type Displacement Sensor used in a Novel Soft Robotic Muscle Actuator,” in 2020 International Conference on Image Processing and Robotics (ICIP), Mar. 2020, pp. 1–6.
2. A. L. Kulasekera, R. B. Arumathanthri, D. S. Chathuranga, T. D. Lalitharatne, and R. C. Gopura, “A Low-Profile Vacuum Actuator: Towards a Sit-to-Stand Assist Exosuit,” in 2020 3rd IEEE International Conference on Soft Robotics (RoboSoft), May 2020, pp. 110–115.
3. Abstract in Conference on Fourth Industrial Revolution and Healthcare -2018

BIBLIOGRAPHY

[1] Michele G. Antonelli, Pierluigi Beomonte Zobel, Francesco Durante, and Terenziano Raparelli. Numerical modelling and experimental validation of a McKibben pneumatic muscle actuator. *Journal of Intelligent Material Systems and Structures*, 28(19):2737–2748, nov 2017.

[2] R.B. Arumathanthri, B.S.K. Abeygoonawardhana, I.D.C.D. Kumarasinghe, D.S. Chathuranga, Thilina Dulantha Lalitharatne, and A.L. Kulasekera. A Soft Robotic Gripper with Sensory Feedback Fabricated by Latex using Coagulant Dipping Process. *2018 IEEE International Conference on Robotics and Biomimetics (ROBIO)*, pages 2082–2087, 2018.

[3] R. Adam Bilodeau, Aslan Miriyev, Hod Lispon, and Rebecca Kramer-Bottiglio. All-soft Material System for Strong Soft Actuators. *IEEE Transactions on Robotics and Automation*, (April), 2018.

[4] Axel Buguin, Min-Hui Li, Pascal Silberzan, Benoit Ladoux, and Patrick Keller. Micro-Actuators: When Artificial Muscles Made of Nematic Liquid Crystal Elastomers Meet Soft Lithography. *Journal of the American Chemical Society*, 128(4):1088–1089, feb 2006.

[5] D G Caldwell and M J Goodwin. Braided Pneumatic Actuator Control of a Multi-Jointed Manipulator. pages 423–428.

[6] Arkadeep Narayan Chaudhury and Debasis Datta. Analysis of prismatic springs of non-circular coil shape and non-prismatic springs of circular coil shape by analytical and finite element methods. *Journal of Computational Design and Engineering*, 4(3):178–191, jul 2017.

[7] Ching-Ping Chou and B Hannaford. Measurement and modeling of McKibben pneumatic artificial muscles. *IEEE Transactions on Robotics and Automation*, 12(1):90–102, 1996.

[8] Nelson Costa and D.G. Caldwell. Control of a Biomimetic ”Soft-actuated” 10DoF Lower Body Exoskeleton. In *The First IEEE/RAS-EMBS International Conference on Biomedical Robotics and Biomechatronics, 2006. BioRob 2006.*, volume 2006, pages 495–501. IEEE, 2006.

[9] Michael F. Cullinan, Eamonn Bourke, Kevin Kelly, and Conor McGinn. A McKibben Type Sleeve Pneumatic Muscle and Integrated Mechanism for Improved Stroke Length. *Journal of Mechanisms and Robotics*, 9(1):011013, jan 2017.

[10] Frank Daerden and Dirk Lefeber. The Concept and Design of Pleated Pneumatic Artificial Muscles. *International Journal of Fluid Power*, 2(3):41–50, jan 2001.

[11] Michael D. Dickey, Ryan C. Chiechi, Ryan J. Larsen, Emily A. Weiss, David A. Weitz, and George M. Whitesides. Eutectic Gallium-Indium (EGaIn): A Liquid Metal Alloy for the Formation of Stable Structures in Microchannels at Room Temperature. *Advanced Functional Materials*, 18(7):1097–1104, apr 2008.

[12] Nicholas Farrow and Nikolaus Correll. A soft pneumatic actuator that can sense grasp and touch. In *2015 IEEE/RSJ International Conference on Intelligent Robots and Systems (IROS)*, volume 2015-Decem, pages 2317–2323. IEEE, sep 2015.

[13] Wyatt Felt. *Sensing Methods for Soft Robotics*. 2017.

[14] Wyatt Felt, Khai Yi Chin, and C. David Remy. Contraction Sensing With Smart Braid McKibben Muscles. *IEEE/ASME Transactions on Mechatronics*, 21(3):1201–1209, jun 2016.

[15] Wyatt Felt, Khai Yi Chin, and C. David Remy. Smart Braid Feedback for the Closed-Loop Control of Soft Robotic Systems. *Soft Robotics*, 00(00):soro.2016.0056, jun 2017.

[16] Wyatt Felt, Shihan Lu, and C. David Remy. Modeling and Design of 'Smart Braid' Inductance Sensors for Fiber-Reinforced Elastomeric Enclosures. *IEEE Sensors Journal*, 18(7):2827–2835, 2018.

[17] Daniel P Ferris, Joseph M Czerniecki, and B Hannaford. An ankle-foot orthosis powered by artificial muscles. *Journal of Applied Biomechanics*, 21:189–197, 2005.

[18] Carter S. Haines, Márcio D. Lima, Na Li, Geoffrey M. Spinks, Javad Foroughi, J. D. W. Madden, Seon H. Kim, Shaoli Fang, M. Jung de Andrade, F. Goktepe, O. Goktepe, Seyed M. Mirvakili, Sina Naficy, X. Lepro, Jiyoung Oh, Mikhail E. Kozlov, Seon Jeong Kim, Xiuru Xu, Benjamin J. Swedlove, Gordon G. Wallace, and Ray H. Baughman. Artificial Muscles from Fishing Line and Sewing Thread. *Science*, 343(6173):868–872, feb 2014.

[19] Blake Hannaford, Jack M. Winters, Ching-Ping Chou, and Pierre-Henry Marbot. The anthroform biorobotic arm: A system for the study of spinal circuits. *Annals of Biomedical Engineering*, 23(4):399–408, jul 1995.

[20] Hugh Herr and Roy Kornbluh. New horizons for orthotic and prosthetic technology : artificial muscle for ambulation. 5385:1–9, 2004.

[21] A Hildebrandt, O Sawodny, D Ilmenau, and Festo Ag. Cascaded control concept of a robot with two degrees of freedom driven by four artificial pneumatic muscle actuators. pages 680–685, 2005.

[22] Lindsey Hines, Kirstin Petersen, Guo Zhan Lum, and Metin Sitti. Soft Actuators for Small-Scale Robotics. *Advanced Materials*, 29(13), 2017.

[23] Jackson Wirekoh and Yong-Lae Park. Design of flat pneumatic artificial muscles. 2016.

[24] Sangbae Kim, Elliot Hawkes, Kyujin Choy, Matthew Joldaz, Joe Foleyz, and Robert Wood. Micro artificial muscle fiber using NiTi spring for soft robotics.

In *2009 IEEE/RSJ International Conference on Intelligent Robots and Systems*, pages 2228–2234. IEEE, oct 2009.

[25] Shunichi Kurumaya, Hiroyuki Nabae, Gen Endo, and Koichi Suzumori. Design of thin McKibben muscle and multifilament structure. *Sensors and Actuators, A: Physical*, 261:66–74, 2017.

[26] Chiwon Lee, Myungjoon Kim, Yoon Jae Kim, Nhayoung Hong, Seungwan Ryu, H. Jin Kim, and Sungwan Kim. Soft robot review. *International Journal of Control, Automation and Systems*, 15(1):3–15, feb 2017.

[27] Carmel Majidi. Soft Robotics: A Perspective—Current Trends and Prospects for the Future. *Soft Robotics*, 1(1):5–11, mar 2014.

[28] Yasuko Matsui, Tetsuya Akagi, and Shujiro Dohta. Development of Flexible Displacement Measuring System Using Wire-type Linear Encoder for Flexible Spherical Actuator. *Procedia Computer Science*, 76(Iris):113–118, 2015.

[29] Gregory Mccarthy, Daniil Effraimidis, Brian Jennings, Nicholas Corso, Cagdas D Onal, and Marko Popovic. Hydraulically Actuated Muscle (HAM) Exo-Musculature.

[30] Yigit Menguc, Yong-Lae Park, Ernesto Martinez-Villalpando, Patrick Aubin, Miriam Zisook, Leia Stirling, Robert J. Wood, and Conor J. Walsh. Soft wearable motion sensing suit for lower limb biomechanics measurements. In *2013 IEEE International Conference on Robotics and Automation*, pages 5309–5316. IEEE, may 2013.

[31] Tissaphern Mirfakhrai, John D.W. Madden, and Ray H. Baughman. Polymer artificial muscles. *Materials Today*, 10(4):30–38, apr 2007.

[32] Mayuko Mori, Koichi Suzumori, Masayuki Takahashi, and Takashi Hosoya. Very high force hydraulic McKibben artificial muscle with a p-phenylene-2,6-benzobisoxazole cord sleeve. *Advanced Robotics*, 24(1-2):233–254, 2010.

[33] John Morrow, Hee-sup Shin, Jacob Torrey, Riley Larkins, Steven Dang, Calder Phillips-grafflin, Yong-lae Park, and Dmitry Berenson. Improving Soft Pneumatic Actuator Fingers through Integration of Soft Sensors , Position and Force Control , and Rigid Fingernails. pages 5024–5031, 2015.

[34] T. Nakamura and H. Shinohara. Position and Force Control Based on Mathematical Models of Pneumatic Artificial Muscles Reinforced by Straight Glass Fibers. *Proceedings 2007 IEEE International Conference on Robotics and Automation*, (April):4361–4366, 2007.

[35] Toshiro Noritsugu, Masahiro Takaiwa, and Daisuke Sasaki. Power assist wear driven with pneumatic rubber artificial muscles. *15th International Conference on Mechatronics and Machine Vision in Practice, M2VIP'08*, pages 539–544, 2008.

[36] Yong-Lae Park, Bor-rong Chen, Carmel Majidi, Robert J. Wood, Radhika Nagpal, and Eugene Goldfield. Active Modular Elastomer Sleeve for Soft Wearable Assistance Robots. In *2012 IEEE/RSJ International Conference on Intelligent Robots and Systems*, pages 1595–1602. IEEE, oct 2012.

[37] Yong Lae Park, Jobim Santos, Kevin G. Galloway, Eugene C. Goldfield, and Robert J. Wood. A soft wearable robotic device for active knee motions using flat pneumatic artificial muscles. *Proceedings - IEEE International Conference on Robotics and Automation*, pages 4805–4810, 2014.

[38] Francesco Rosso, Gerardo Marino, Antonio Giordano, Manlio Barbarisi, Domenico Parmeggiani, and Alfonso Barbarisi. Smart materials as scaffolds for tissue engineering. *Journal of Cellular Physiology*, 203(3):465–470, jun 2005.

[39] Daniela Rus and Michael T. Tolley. Design, fabrication and control of soft robots. *Nature*, 521(7553):467–475, 2015.

[40] Norihiko Saga, Taro Nakamura, and Kenji Yaegashi. Mathematical model of pneumatic artificial muscle reinforced by straight fibers. *Journal of Intelligent Material Systems and Structures*, 18(2):175–180, 2007.

[41] Min-Geun Sang Yul Yang1, Kyeong Ho Cho1, Youngeun Kim1, Ja Song2, Ho Sang Jung1, Ji Wang Yoo3, Hyungpil Moon1, Jae-do Nam3 Choon Koo1, and Hyouk Ryeol Choi1. High performance twisted and coiled soft actuator with Spandex fiber for artificial muscles. 2018.

[42] Daisuke Sasaki, Toshiro Noritsugu, and Masahiro Takaiwa. Development of active support splint driven by pneumatic soft actuator (ASSIST). *Proceedings - IEEE International Conference on Robotics and Automation*, 2005(April):520–525, 2005.

[43] Saivimal Sridar, Corey J Majeika, Phillip Schaffer, Matthew Bowers, Seiichiro Ueda, Andrew J Barth, Jon L Sorrells, Jon T Wu, Thane R Hunt, and Marko Popovic. Hydro Muscle – A Novel Soft Fluidic Actuator. pages 4014–4021, 2016.

[44] Yi Sun, Jin Guo, Tiana Monet Miller-jackson, Xinquan Liang, Marcelo H Ang Jr, Raye Chen, and Hua Yeow. Design and Fabrication of a Shape-Morphing Soft Pneumatic Actuator : Soft Robotic Pad. pages 6214–6220, 2017.

[45] Texas Instruments. *LDC1612, LDC1614 Multi-Channel 28-Bit Inductance to Digital Converter (LDC) for Inductive Sensing*, 2018.

[46] N.G. Tsagarakis and Darwin G. Caldwell. Development and Control of a 'Soft-Actuated' Exoskeleton for Use in Physiotherapy and Training. *Autonomous Robots*, 15(1):21–33, 2003.

[47] Kosuke Tsuneyasu, Ayumu Ohno, Yoshiyuki Fukuda, Kazunori Ogawa, Toshio Tsuji, and Yuichi Kurita. A soft exoskeleton suit to reduce muscle fatigue with pneumatic artificial muscles. 2018.

[48] Shuichi Wakimoto, Koichi Suzumori, and Takefumi Kanda. Development of intelligent McKibben actuator. In *2005 IEEE/RSJ International Conference on Intelligent Robots and Systems*, pages 487–492. IEEE, 2005.

[49] Shuichi Wakimoto, Koichi Suzumori, and Takefumi Kanda. DEVELOPMENT OF INTELLIGENT MCKIBBEN ACTUATOR WITH BUILT-IN SOFT CONDUCTTVE RUBBER SENSOR. In *2005 IEEE/RSJ International Conference on Intelligent Robots and Systems*, pages 487–492. IEEE, 2005.

[50] Zhongkui Wang, Damith Suresh Chathuranga, and Shinichi Hirai. 3D printed soft gripper for automatic lunch box packing. In *2016 IEEE International Conference on Robotics and Biomimetics (ROBIO)*, pages 503–508. IEEE, dec 2016.

[51] Yong-Lae Park, Bor-Rong Chen, and Robert J. Wood. Design and Fabrication of Soft Artificial Skin Using Embedded Microchannels and Liquid Conductors. *IEEE Sensors Journal*, 12(8):2711–2718, aug 2012.

[52] Aaron J. Young and Daniel P. Ferris. State of the art and future directions for lower limb robotic exoskeletons. *IEEE Transactions on Neural Systems and Rehabilitation Engineering*, 25(2):171–182, 2017.

[53] Yanlei Yu and Tomiki Ikeda. Soft Actuators Based on Liquid-Crystalline Elastomers. *Angewandte Chemie International Edition*, 45(33):5416–5418, aug 2006.

[54] Michelle C Yuen, Rebecca Kramer-bottiglio, and Jamie Paik. Strain Sensor-Embedded Soft Pneumatic Actuators for Extension and Bending Feedback. 2018.

APPENDIX A

FIRST APPENDIX

```
#include "LDC16xx_lib.h"

int in = 4;
int out = 5;
float distance = 0;
float setpoint = 0;
float L = 0;
float initialL=0;
boolean first = false;
float increment = 10;
float ind_increment=0;
float ind_gap = 1*0.0025;
float height=0;
unsigned long time1;
unsigned long t;


unsigned long start;
bool switch1=true;
int timegap = 2000;
```

```
// user selecatable comppile option
// 0 - use user polling to read sensor data
// 1 - use syncronized sensor read with INTB pin interrupt
#define IRQ_HANDLER 0

// single channel conversion setup with disabled INTB by default
LDC_configReg default_config[] = {
{ LDC16xx_MUX_CONFIG,0x020f },
{ LDC16xx_CONFIG,LDC16xx_BITS_ACTIVE_CHAN_CH0 |
 LDC16xx_BITS_AUTO_AMP_DIS | LDC16xx_BITS_INTB_DIS },
{ LDC16xx_SETTLECOUNT_CH0,0x0000 },
{ LDC16xx_RCOUNT_CH0, 0x0080 },
};

#define LDC_CONFIG_SIZE
sizeof(default_config)/sizeof(LDC_configReg)

// global sensor object pointer
LDC16xx *ldc;

// an ISR control flag for pending sensor data
volatile bool drdy = 0;

// interrupt service routine-when sensor conversion is complete
// this code should be light not to block the main
loop for too long
void onDataReady(){
drdy = true;
}
```

```
void setup() {
pinMode(in ,OUTPUT);
pinMode(out,OUTPUT);

// put your setup code here, to run once:

Serial.begin(115200);
start = millis();

Serial.println("Starting execution ...");

// create a new LDC sensor object, initialize interface
// I2C clock of 100kHz or 400kHz is allowed
ldc = new LDC16xx(Wire, 400000);

// verify chip ID. On fail halt program
uint16_t id, manuf;
ldc->readRegister(LDC16xx_DEVICE_ID, &id);
ldc->readRegister(LDC16xx_MANUFACTURER_ID, &manuf);

Serial.print("Chip ID: 0x");
Serial.println(id, HEX);
Serial.print("Manufacturer ID: 0x");
Serial.println(manuf,HEX);

if(id == LCD16xx_DEFAULT_DEVICE_ID &&
manuf == LDC16xx_DEFAULT_MANUFACTURER_ID){
Serial.println("Verification OK");
} else {
Serial.println("Wrong chip or manufacturer ID,
```

```
stopping execution..");
while(1);
}

// reset device wiping previous configuration
ldc->resetDevice();

// load our config
ldc->loadConfig(default_config, LDC_CONFIG_SIZE);

#if IRQ_HANDLER == 1
// attach IRQ and set appropriate LDC
registers to enable INTB interrupt
// user pin 2 for INTB
ldc->enableDataReadyInterrupt(2, onDataReady);
#endif

// for debug, dump values of all register to the console
ldc->registerDump(Serial);
digitalWrite(out , HIGH);
delay(5000);
digitalWrite(out , LOW);

digitalWrite(in , HIGH);
delay(100);
digitalWrite(in , LOW);
delay(500);
analogWrite(A0,200);
delay(100);
analogWrite(A0,0);
```

```
}

// main loop

//time1 = millis();

void loop() {
t = millis();

if((millis() - start) >=timegap){
if(switch1){
height=0.81;
}else{
height=0.76;
}
switch1 = ! switch1;
start = millis();
}
//  Serial.println(height);
delay(10);


main1();

}

void main1(){
#if IRQ_HANDLER == 1
while(!drdy);
drdy = false;
```

```
#endif

uint32_t data;
uint16_t status;

// read the channel no 0. data
ldc->readChannel(0, &data);

#if IRQ_HANDLER == 1
// in IRQ mode status must be read to re-enable conversion
and re-assert INTB
ldc->readRegister(LDC16xx_STATUS, &status);
#endif

// print read data in the console
//Serial.println(data, DEC);
float d = float(data/10000);
L = 9690000/(d*d);
//    Serial.print(L);

control();



#if IRQ_HANDLER == 0
// we time the loop by ourselves
(optionally we could ask the chip periodically for status)
// ideally you should make sure we are syncronized with sensor
conversion rate (RCOUNT + clock source)
delay(24); // ~41.5 sps
#endif
```

```
}



void control(){

//L = 0.0022D+0.75
//distance = ((L-0.75)/0.0022);




if( first == false ){
delay(20);
initialL=L;
//setpoint = initialL + ind_increment;
first = true;
}

increment=0+height;

//ind_increment= increment*0.0025;

ind_increment= increment;
setpoint = ind_increment;


Serial.print(",");
Serial.print(L);
```

```
Serial.print(",");
Serial.print(height);
Serial.print(",");
Serial.print((L-initialL)*400);
Serial.print(",");
Serial.println(setpoint);

/*
digitalWrite(in,LOW);
delay(1000);
digitalWrite(in,HIGH);
delay(1000);
*/




if ( L >= (setpoint) ){
digitalWrite(in,LOW);
digitalWrite(out,HIGH);
delay(1);
}

else if ( L <= (setpoint) ){
digitalWrite(in,HIGH);
digitalWrite(out,LOW);
delay(1);
}
```

```
else{
digitalWrite(in,LOW);
digitalWrite(out,LOW);
delay(5);
}
}
```